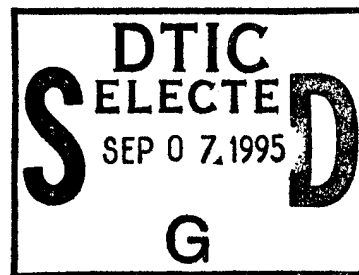


Heteroepitaxial Diamond Growth

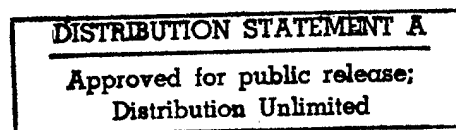
Third Quarterly Report
1 July 1994- 30 September 1994



Submitted to
Ballistic Missile Defense Organization
Innovative Science and Technology Office
Office of Naval Research
Program No. N00014-92-C-0081

Prepared by
Research Triangle Institute

19950905 030



83U-5294
September 1995

DTIC QUALITY ASSURED



REPORT DOCUMENT PAGE

Form Approved
OMB No 0704-0188

Public reporting burden for this collection of information is estimated to average 1 hour per response, including the time for reviewing instructions, searching existing data sources, gathering and maintaining the data needed, and completing and reviewing the collection of information. Send comments regarding this burden estimate or any other aspect of this collection of information, including suggestions for reducing this burden to Washington Headquarters Services, Directorate for Information Operations and Reports, 1215 Jefferson Davis Highway, Suite 1204 Arlington, VA 22202-4302, and to the Office of Management and Budget Paperwork Reduction Project (0704-0188), Washington, DC 20503.

1. AGENCY USE ONLY (Leave blank)

2. REPORT DATE

September 1995

3. REPORT TYPE AND DATES COVERED

Quarterly Report

1 July 1994 -- 30 September 1994

4. TITLE AND SUBTITLE

Heteroepitaxial Diamond Growth

5. FUNDING NUMBERS

N00014-92-C-0081

6. AUTHOR(S)

R. J. Markunas, R. A. Rudder, J. B. Posthill, R. E. Thomas, G. Hudson

7. PERFORMING ORGANIZATION NAME(S) AND ADDRESS(ES)

Research Triangle Institute
P. O. Box 12194
Research Triangle Park, NC 27709

8. PERFORMING ORGANIZATION
REPORT NUMBER

83U-5294

9. SPONSORING/MONITORING AGENCY NAME(S) AND ADDRESSES(ES)

Office of Naval Research
800 N. Quincy Street
Arlington, VA 22217-5000

10. SPONSORING/MONITORING
AGENCY REPORT NUMBER

11. SUPPLEMENTARY NOTES

12a. DISTRIBUTION/AVAILABILITY STATEMENT

Approved for public release; unlimited distribution

12b. DISTRIBUTION CODE

13. ABSTRACT

Progress in the quarter was primarily in the area of optimization of homoepitaxial diamond. Since this is in the critical path for a large-area single-crystal diamond technology, a focused effort to identify and eliminate topographical asperities from epi surfaces was undertaken. The source of the problem was found to be the reactor configuration and growth protocols, and these areas were addressed. Excellent state-of-the-art homoepitaxial CVD diamond is now being grown at RTI using water/alcohol mixtures. Additionally, more details on our tiling (epitaxial joining) and NEA surface activation have been published and submitted for publication.

14. SUBJECT TERMS

15. NUMBER OF PAGES

16. PRICE CODE

17. SECURITY CLASSIFICATION
OF REPORT

UNCLASSIFIED

18. SECURITY CLASSIFICATION
OF THIS PAGE

UNCLASSIFIED

19. SECURITY CLASSIFICATION
OF ABSTRACT

UNCLASSIFIED

20. LIMITATION OF ABSTRACT

TABLE OF CONTENTS

| | |
|---|---|
| 1.0 INTRODUCTION | 1 |
| 2.0 DIAMOND HOMOEPITAXIAL GROWTH OPTIMIZATION | 2 |
| 2.1 Background | 2 |
| 2.2 Diamond Substrate and Surface..... | 2 |
| 2.3 Diamond Homoepitaxy..... | 2 |
| 3.0 PUBLICATIONS | 8 |

| | |
|----------------------|-------------------------------------|
| Accession For | |
| NTIS CRA&I | <input checked="" type="checkbox"/> |
| DTIC TAB | <input type="checkbox"/> |
| Unannounced | <input type="checkbox"/> |
| Justification | |
| By | |
| Distribution / | |
| Availability Codes | |
| Dist | Avail and / or Special |
| A-1 | |

Quarterly Report Third Quarter

1 July 1994- 30 September 1994

1.0 INTRODUCTION

This is the 1994 third quarterly report on the Heteroepitaxial Diamond Growth Program Contract No. N-00041-92-C-0081.

Work progressed in one major area this quarter: improvement of diamond homoepitaxy. The ability to do excellent, routine diamond homoepitaxy is in the critical path for *any* large-area single-crystal diamond technology. It is a cornerstone of our efforts to produce a large-area single-crystal diamond substrate via a tiled array. This progress in CVD growth of homoepitaxial diamond is described herein. Additionally, we have summarized our tiled array (epitaxial joining) work by publishing two papers in the open literature. Another manuscript was submitted for publication that gives our current interpretation on the role of hydrogen on the negative electron affinity (NEA) diamond surface. These manuscripts are included in this report.

2.0 DIAMOND HOMOEPITAXIAL GROWTH OPTIMIZATION

2.1 Background

In the 1992-1993 timeframe, we had considerable difficulty and inconsistency with our diamond homoepitaxial growth process (see Fig. 1 for example). This represented a huge problem that had to be solved so as to enable the development of a large-area diamond single-crystal technology *regardless* of whether a heteroepitaxial or homoepitaxial (tiling/epitaxial joining) method proved to be the most viable route to success. Since the source of such difficulties was unclear, we embarked on two simultaneous routes to pinpoint the problem and solve it:

1. Focus on the starting single-crystal diamond substrate and surface.
2. Focus on the diamond deposition process.

As is self-evident, these two potential sources of difficulty cannot be experimentally deconvolved, hence the need to approach both simultaneously.

2.2 Diamond Substrate and Surface

For this potential problem, we embarked on a series of experiments that involved different surface cleaning treatments (see Final Report 1993, this project, Feb. 1994). The results were not conclusive, leading us to believe that if the substrates were the essence of the problem, a more severe "fix" was necessary. We then attempted to remove surface layers via implantation, annealing, electrochemical etching and plasma treatments (see First Quarterly Report 1994, this project, September 1994). This met with some success, but it appeared that the surface treatments were not the ultimate bottleneck in obtaining high-quality homoepitaxial diamond.

2.3 Diamond Homoepitaxy

Simultaneously, we began "tuning" our diamond homoepi CVD process. A number of changes were made to our primary diamond CVD reactor:

- New gas delivery package
- Liquid mass flow controllers

A



B

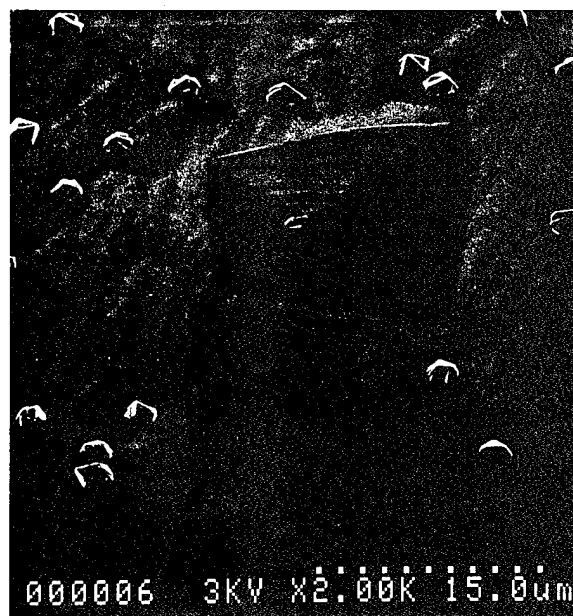


Figure 1: Two examples of diamond homoepitaxial (100) growth runs that indicated serious problems: (a) cleaning the substrate involved ethanol/water jet growth using CH_4/H_2 gas mixture and (b) no substrate cleaning; growth using $\text{CO}/\text{CH}_4/\text{H}_2$ gas mixture.

- New, heated lines
- New tanks
- Rebuilt heater/new tube
- Mo sample holder
- Installation and routine use of RGA

It is believed that these changes enable a greater degree of control over the gas phase composition during growth while using water/alcohol growth chemistries.

Additionally, we developed other protocols for diamond growth that were subsequently optimized for homoepitaxial diamond growth specifically. They are:

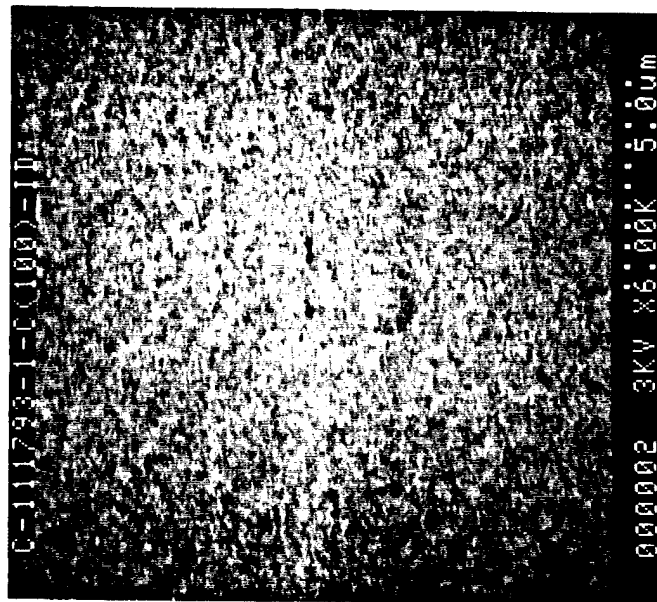
- Pre-coat the Mo sample holder.
- Preheat diamond sample to $\sim 600^{\circ}\text{C}$.
- Establish ethanol and water flows at 18 sccm and 12 sccm respectively.
- Maintain pressure at 1 Torr.
- Strike discharge.
- Reduce filament heater to keep sample at $\sim 600^{\circ}\text{C}$.

We found that the epitaxial growth rate was $\cong 0.5 \mu\text{m/hr}$ using these conditions. Figure 2 shows smooth surface topographies from the same sample after one hour of growth and after sixteen hours of growth. The diamond homoepitaxial surfaces are smooth, and we have found that they can remain smooth to the maximum time that we have attempted growth thus far (150 hours $\cong 75 \mu\text{m}$ thickness). No cracking has ever been seen in our homoepitaxial films grown as described above. Figure 3 shows etch pit delineations in some of our homoepitaxial films of different thicknesses grown on C(100) type Ia substrates. It appears that densities are in the mid -10^5cm^{-2} to low -10^6cm^{-2} range.

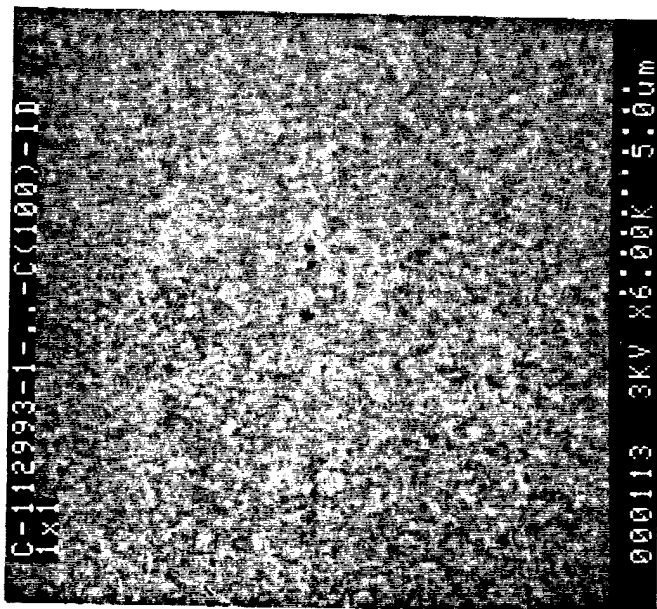
From the above results, we have concluded that our original problem was with our growth reactor and protocols, and we have been able to overcome them to grow state-of-

the-art homoepitaxial films using water/alcohol source chemistries at low temperature (~600°C).

SEM OF DIAMOND HOMOEPI TAXY ON AS-RECEIVED
C(100) TYPE Ia SUBSTRATES



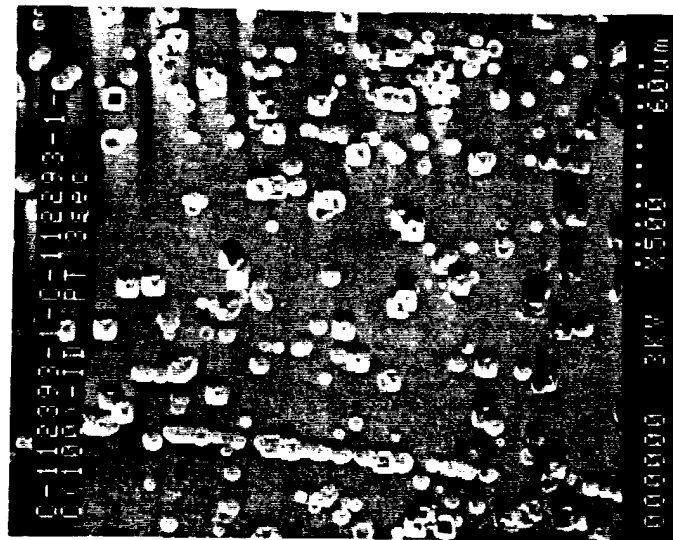
Growth: t = 1 hr.



Growth: t = 16 hrs.

Figure 2

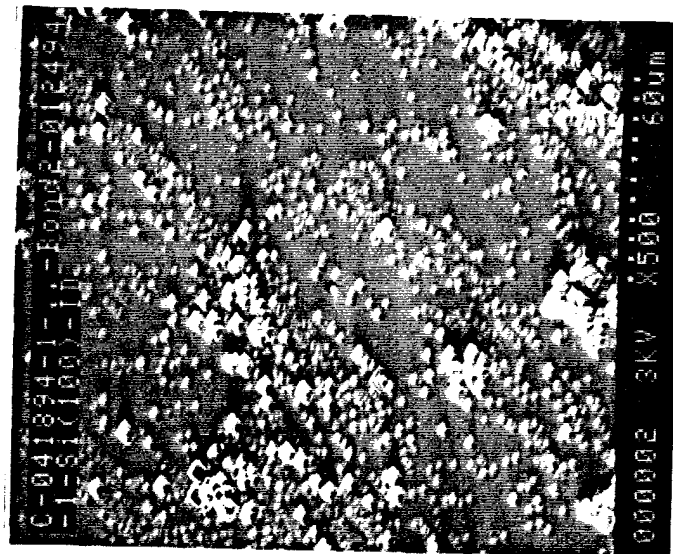
DEFECT DELINEATION VIA PROPANE TORCH IN DIFFERENT HOMOEPITAXIAL DIAMOND FILMS GROWN ON C(100) TYPE Ia SUBSTRATES



$t = 8$ hrs.
 $h \approx 4 \mu\text{m}$
 $\rho \approx 7 \times 10^5 \text{ cm}^{-2}$



$t = 26.5$ hrs.
 $h \approx 13 \mu\text{m}$
 $\rho \approx 6 \times 10^5 \text{ cm}^{-2}$



$t = 154.5$ hrs.
 $h \approx 75 \mu\text{m}$
 $\rho \approx 2 \times 10^6 \text{ cm}^{-2}$

Figure 3

3.0 PUBLICATIONS

1. J. B. Posthill, D. P. Malta, G. C. Hudson, R. E. Thomas, T. P. Humphreys, R. C. Hendry, R. A. Rudder, and R. J. Markunas, *Demonstration of a Method to Fabricate a Large-Area Diamond Single-Crystal*, Thin Solid Films, accepted for publication, 28 June 1995.
2. D. P. Malta, J. B. Posthill, G. C. Hudson, R. E. Thomas, T. P. Humphreys, R. A. Rudder, and R. J. Markunas, *Process of Epitaxial Joining to Fabricate a Large-Area Diamond Single-crystal*, presented and published, 1995 Electrochemical Society Meeting, Reno, NV.
3. T. P. Humphreys, R. E. Thomas, D. P. Malta, J. B. Posthill, M. J. Mantini, R. A. Rudder, G. C. Hudson, *Enhancement of Secondary Electron Emission from C(001)*, submitted to Appl. Phys. Lett.

DEMONSTRATION OF A METHOD TO FABRICATE A LARGE-AREA DIAMOND SINGLE CRYSTAL

J.B. Posthill, D.P. Malta, G.C. Hudson, R.E. Thomas, T.P. Humphreys,
R.C. Hendry, R.A. Rudder, and R.J. Markunas

Research Triangle Institute, Research Triangle Park, North Carolina 27709-2194 USA

Abstract

A multi-step process to fabricate a diamond single crystal that is larger than the original, natural, commercially-obtained crystals is described. Starting with 3.0mm×3.0mm×0.25mm, natural, type Ia C(100) crystals that have had their edges oriented to (010) and (001), we have successfully bonded two to a Si substrate in close proximity to each other. Subsequent diamond homoepitaxy using plasma-enhanced chemical vapor deposition of up to ~75μm thickness has enabled epitaxial overgrowth to join the two diamonds. The topography was excellent, and microRaman spectroscopy indicated only a 0.6 cm⁻¹ line broadening (crystal degradation) at the joint. The creation of etch pits (via oxidizing flame) on the joined diamond surface indicated a higher defect density at the joint, but this more defective region was constrained to within the dimension of the original gap between the diamond crystals. These results indicate that this process of epitaxial joining of diamond single crystals has the potential to be scaled up to larger area in order to fabricate a diamond single crystal of desired area and reasonable crystal perfection.

Accepted for publication

28 June 1995

Thin Solid Films

1. Introduction

The search for and trade in large diamond single crystals has interested segments of the international free market for centuries. There is a limited supply of natural diamonds due to the unique geological conditions required for their formation, and large diamond single crystals of high crystal perfection are correspondingly even more rare. Combined with diamond's innate desirability and attractiveness as gemstones, it is not surprising that the great majority of large diamond single crystals are too expensive to be considered for extensive technological applications. However, the technological attractiveness of diamond is increasing due to diamond's several unique and extreme properties [1]. This has led to considerable research into synthetically-produced diamond. High pressure, high temperature (HPHT) produced diamond, including single crystal diamond, has already found many technological applications world-wide. Additionally, diamond deposited from the vapor phase has attracted interest sufficient to make this subset of the diamond research field very visible and active in recent years.

Polycrystalline diamond chemical vapor deposition (CVD) research and development has focused on heat sinks, cutting tools, and abrasion-resistant and other types of coating applications [2]. Another goal for many investigators has been to develop a method to fabricate large area single crystal diamond for active diamond-based electronics to take advantage of diamond's novel semiconducting properties [3]. Although electronic devices are being fabricated in polycrystalline diamond [4, 5], it is likely that diamond-based electronics will not reach full potential and theoretical performance until these devices can be fabricated in single crystal material. There might also be other applications for diamond single crystal wafers if they could be produced in a cost-effective manner. Current efforts employing diamond CVD to develop a process to make diamond single crystal films fall into one of two categories: (1) diamond heteroepitaxy on a non-native single crystal substrate using a diamond CVD process, or (2) orienting individual diamonds and epitaxially joining them with a diamond CVD process.

Developing a heteroepitaxial diamond process has been difficult, but there has been some recent progress. In particular, diamond has thus far been grown heteroepitaxially on 100-300 μ m-

size c-BN single crystals [6, 7], BeO single crystals [8], and Ni single crystals [9]. These results were verified by electron microscopy. Diamond has also been grown heteroepitaxially (or in a condition of oriented polycrystalline growth) on SiC single crystals [10] and on Si single crystals [e.g., 11]. Again, these results have been verified by electron microscopy and/or X-ray diffraction texture analysis. Efforts are underway to improve these heteroepitaxial diamond processes in order to increase the quality (lower the defect density) of the diamond layers.

The process of epitaxially joining individual diamond crystals has also met with a degree of success. The essence of this approach is to use a diamond CVD process that will permit good quality homoepitaxial diamond to be grown on multiple diamond crystals that have been crystallographically oriented as closely as possible on a non-native substrate. Underlying this approach is prior research in this laboratory which demonstrated that epitaxial diamond could be grown laterally and vertically at comparable rates [12]. Geis, et al. have specially patterned Si(100) wafers in order to hold small ($< 100\mu\text{m}$), similarly-faceted seed diamonds in an array of {111}-faceted pyramidal pits in the Si [13]. This approach enabled the seed diamonds to be held in close proximity to one another and it minimizes the crystallographic misorientation from seed to seed. After growing $\sim 240\mu\text{m}$ of CVD diamond on such a unique structure, a large-area mosaic diamond film was created. Another version of this method, also referred to as mosaic growth of diamond by Janssen and Giling, involves starting with considerably larger diamond single crystals (type IIa, $2\text{mm} \times 2\text{mm}$) that have had their edges and faces oriented and polished to (100) (the faces were actually oriented to 5° off (100) towards [010]) [14, 15]. Two diamond crystals were soldered in close proximity to each other onto a Mo substrate and placed in a hot filament diamond CVD reactor. Growth conditions were used that were previously optimized for (100) homoepitaxial diamond growth. Although this process will require refinement, it does appear that the diamonds have been joined epitaxially at the joint (or gap) between them.

We describe herein our own demonstration of an alternative method of epitaxially joining two diamond single crystal substrates to form a larger area crystal. It is envisaged that such a process, once scaled to larger area, may one day form the basis of a bulk (or boule) diamond

technology which, when combined with appropriate diamond growth, cutting, and polishing techniques, might be used to manufacture single crystal diamond wafers.

2. Experimental Procedure and Development of Process of Epitaxial Joining

To successfully epitaxially join multiple diamond single crystals, several issues had to be addressed. These interrelated issues include:

1. Procuring single crystal diamonds that can be crystallographically oriented with respect to each other within a specified misorientation and which are also compatible with good quality diamond homoepitaxial growth.
2. Establishing a reliable homoepitaxial diamond CVD process.
3. Choosing a substrate and verifying the methodology to bond the diamonds to it.
4. Ensuring that the substrate and bonding scheme are compatible with the homoepitaxial diamond CVD process.

Each of these issues and the approach used to address them are described below.

Single Crystal Diamonds

These can be procured commercially, and the options are types Ia, Ib, IIa, and IIb in the crystallographic orientation that is most likely to yield the highest quality homoepitaxial diamond. Based on previous investigations in our laboratory, we have found that natural type Ia diamonds, in spite of the presence of a high density of small nitrogen platelets, contain the lowest dislocation densities and appear to permit reasonable quality (100) homoepitaxial diamond to be grown on them [16, 17]. Additionally, it is necessary to have a means to position each diamond single crystal as closely as possible to the same crystallographic orientation to minimize the creation of low angle boundaries and dislocation formation at the epitaxially joined seams. This was accomplished by requesting the vendor to cut and polish the edges of each of the (100) diamonds on the remaining {010} planes. Therefore, we could use simple abutment of the crystal edges whilst bonding them to a flat surface to achieve a degree of crystallographic registry. It was requested that these {100} orientations be maintained within a tolerance of $\pm 2^\circ$. It was also

believed appropriate to specify a tolerance on the dimensions of the crystals to make the fitting together of crystals (tiling) easier and to minimize the height differences between growth faces of the crystals. The dimensional specifications of the diamond crystals used in this epitaxial joining study were: $3.00 \pm 0.01 \text{ mm} \times 3.00 \pm 0.01 \text{ mm} \times 0.250 \pm 0.005 \text{ mm}$, although diamond crystals of other dimensions, different crystallographic edge orientations, and less rigorous tolerances were also used to develop and test the necessary steps in this process.

Homoepitaxial Diamond CVD

An rf-driven plasma enhanced CVD process that utilizes water and alcohol (ethanol) to grow the homoepitaxial films was used in this study. The use of alcohol/water mixtures for diamond growth was pioneered in our laboratory [18], and the development and details of this homoepitaxial diamond deposition process are described elsewhere [19, 20]. Briefly, the conditions of homoepitaxial diamond growth used were: Reactant flow was 18 sccm ethanol and 12 sccm water; Pressure = 1 Torr; Power (rf) $\cong 1.5 \text{ kW}$; Growth temperature $\cong 600^\circ\text{C}$; Growth rate $\cong 0.5 \mu\text{m-hr}^{-1}$. Run times were kept $\leq 8 \text{ hr.}$ in order to inspect periodically the progress of homoepitaxial growth and epitaxial joining.

Substrate and Bonding Methodologies

Several preliminary attempts were made with individual and multiple diamond arrangements and different substrates. It was decided initially to utilize a deposited Ni layer on the diamond to act as an intermediate layer in order to bond the diamond to a different, non-native substrate. We previously had developed a process of growing Ni heteroepitaxial films on diamond using e-beam molecular beam epitaxy (MBE), which we used throughout this study [21]. Fig. 1 shows the relatively smooth topography of one such film, grown to a thickness of 128 nm, and Rutherford backscattering(RBS)/channeling results indicating that the film is epitaxial and of reasonable crystalline quality. It is interesting to note that Ni is not a carbide former [22], but it does have a face-centered cubic (fcc) lattice with a lattice parameter of $a_0(\text{Ni}) = 0.3524 \text{ nm}$. This compares favorably with the lattice parameter of diamond [$a_0(\text{C}) = 0.3567 \text{ nm}$], yielding a lattice mismatch of: $f = -1.2\%$. Different thicknesses of Ni heteroepitaxy on diamond were

investigated, and they varied between 100 nm to up to $\sim 3.5\mu\text{m}$. Initial attempts to bond Ni-coated diamonds included: (1) bonding them to themselves to establish that Ni layers can be diffusion bonded, (2) bonding them to Ni(100) substrates, (3) bonding them to Au/W/SiO₂/Si(100) wafers, and (4) bonding them directly to Si(100) wafers. In all cases, we found that bonding could be accomplished by application of a compressive load during heating in flowing N₂ or Ar. No special preparation of the Ni (or Au) surfaces was required to effect bonding when temperatures were as high as 900°C.

Scanning electron microscopy (SEM) results from the cleaved cross-section between two Ni-coated diamonds ($\sim 3.5\mu\text{m}$ of Ni on each) that were bonded in compression at 900°C for 30 min. in flowing N₂ show no large voids or asperities in the bonded region. Since it requires considerable force to cleave these diamonds of 0.25mm thickness, the fact that the joint remained intact upon cleaving indicates the robust nature of the joint. This result led to an attempt to bond to a specially prepared Ni(100) substrate crystal [23]. The crystal was electropolished such that it appeared to have a mirror-smooth finish to the unaided eye. Additionally, the $[010]_{\text{Ni}}$ direction was determined via back reflection Laue X-ray diffraction and scribed onto the crystal so that the diamond $[010]$ edge could be aligned with it. This would then give an opportunity for the Ni heteroepitaxial layer to potentially crystallographically align with the Ni(100) substrate in a cube-cube orientation relationship to minimize the interfacial energy. The Ni-coated diamonds were placed on the Ni(100) surface in close proximity to each other and rotationally aligned as described above. Under a compressive load, this structure was heated to 900°C for 30 min. in flowing N₂ (Fig. 2). It was noted that the underlying Ni(100) crystal deformed, but the Ni-Ni joint was robust enough to withstand transportation and handling. Interestingly and in the context of not applying a longitudinal load while applying the initial compressive load, the diamonds ended up with only a $10\mu\text{m}$ gap between them. This was considered a very impressive result, as it appeared likely that such a small gap could be bridged using a diamond homoepitaxial growth process.

Ni-coated diamonds were also bonded to Si(100) wafers that had been specially metallized. An approach involving Au termination was explored because of the ease in which Au and Ni could alloy would potentially lead to good bonding. Since Au forms a low melting point eutectic with Si, it was necessary to prevent them from coming into contact with each other. Plasma-enhanced CVD oxide was deposited on Si(100) wafers to a thickness of 50nm [24] followed by sputtering a small amount of W (~ 5nm) to promote adhesion. Then 2 μ m of Au was evaporated onto the wafers. A special fixture was made to put a compressive load on the diamond while also being able to push together the diamonds with a longitudinal load. Additionally, it was possible to view the top surface of the diamonds through a window in the furnace and the sapphire substrate that bore down on the top of the diamonds. Upon heating such a structure in flowing Ar, it was possible to see, with the unaided eye, the reaction between the Au and Ni. The reaction moved in a front, and when complete, the furnace was turned off. It was a continuous process that was observed to begin once the fixture reached ~ 750°C and was completed about 10 min. later when the fixture reached approximately 850°C. Robust diamond to Si wafer bonding was thereby achieved. This is shown in Fig. 3 where a tiled array consisting of four 3.0mm \times 3.0mm diamonds was made. In some areas, the gap between diamonds was as little as 1.5 μ m, but this was not perfectly uniform.

Bonding Ni-coated diamonds to Si(100) directly was then investigated. For this process, it was found desirable to deposit heteroepitaxial Ni \geq 2 μ m thick. A different fixture was designed and built which loaded two diamonds in compression normal to the face while simultaneously loading them longitudinally to minimize the gap between them. This is shown schematically in Fig. 4. Fig. 5 shows how extensive the reaction is when a Ni-coated diamond (2 μ m of heteroepitaxial Ni) is pressed onto a Si wafer and heated to 900°C over the period of 1 hr. in flowing Ar. Upon cooling, a diamond was pried off the surface; showing a rough and irregular fracture surface that indicates brittle failure. Another diamond/Ni/Si structure is shown in cross-section (Fig. 5b). Interestingly, the region labeled "Ni(100)" in the micrograph is found to be ~ 7 μ m thick -- well beyond the original 2 μ m Ni thickness. It is clear that there has been solid state

reaction between the Si and the Ni, with perhaps some of the diamond also getting consumed. Initial results from energy dispersive X-ray spectroscopy (EDS) using an SEM indicated that there were two distinct layers within the $\sim 7\mu\text{m}$ reacted region that differed in composition -- in particular the Si:Ni ratio. Not surprisingly, the lower portion contains a higher Si:Ni ratio than the upper portion. However, the EDS detector used was fitted with a Be window detector, therefore light element analysis ($Z < 12$) was precluded. Electron microprobe analysis using wavelength dispersive spectrometry (WDS) was also difficult with regard to carbon detection because secondary x-ray fluorescence of the nearby diamond gave inflated carbon values. Calculating the carbon concentration by subtracting the measured Si and Ni concentrations (as determined by yield) from 100%, gave the results shown in Table 1. It is interesting that there is not a significant difference in carbon concentration between the layers, but there is a difference between the Si:Ni ratios similar to that observed qualitatively in the EDS spectra. To the best of our knowledge, there are no known phases with these listed compositions, and it might be that each layer has multiple phases contained within them. Perhaps the most surprising thing about these results is the degree to which carbon from the diamond has been incorporated in this reacted region. Clearly, all three elements in the original diamond/Ni/Si structure have indeed participated in the bonding process, and, perhaps, this is responsible for the robust diamond to Si adhesion that is observed. When bonding two diamonds side by side for epitaxial joining using this process, bond gaps did vary from as little as $\sim 4\mu\text{m}$ to as much as $\sim 50\mu\text{m}$.

Compatibility with Diamond CVD Process

Diamonds bonded to Ni(100) substrates and Au/W/SiO₂/Si(100) substrates were unfortunately found to be incompatible with the diamond homoepitaxial CVD process. In the growth on diamonds on Ni(100), it is believed that the large amount of Ni that is directly exposed to the plasma "poisons" the growth process. This is consistent with initial attempts in our laboratory at polycrystalline/epitaxial diamond growth on Ni surfaces, where even diamond scratching to promote nucleation appears to do little to mitigate the formation of graphite on the Ni surface [25]. The Au-terminated Si(100) wafers also had problems in the CVD process. The

Au appears to be stripped from the exposed portions of the sample, which was associated with a very poor growth topography on the diamond. One possibility with the metal or metal-terminated substrates is that the metal may be getting heated well beyond the nominal temperature of growth due to inductive coupling from the rf drive. Also, the sample (diamonds bonded to substrate) can be seen to be immersed in the plasma, thereby ensuring a high degree of atomic collisions with the surface. Both of these factors (vapor pressure and sputtering) may contribute to the loss of metal into the vapor phase, which could effect adversely the growth process. In any case, these two metals appear to be incompatible with the water/alcohol, homoepitaxial diamond CVD process used in this study.

Use of the diamond bonded to Si samples faired significantly better. Although Ni is still used, it is in small quantities and is incorporated in the reacted region between the diamonds and Si(100) wafer. Also, the Ni is not directly exposed to the plasma. The first attempt at epitaxial joining with two diamonds bonded to Si(100), where the gap between the diamonds was $\sim 4\mu\text{m}$, was successful. A series of four hour diamond growth runs (nominal thickness increase $\sim 2\mu\text{m}$ for each run) was done and the sample was examined in the SEM after each run. Fig. 6 shows some of the micrographs taken from the time-elapsd series. Note that after the first run (first $\sim 2\mu\text{m}$), the diamond topography away from the gap looks reasonably smooth, but at the gap the topography looks disrupted and irregular. However, after 16 total hours of growth ($\sim 8\mu\text{m}$ total), epitaxial joining has been achieved and a step is seen in the approximate location of the gap. Additionally, aside from the step itself, the epitaxially joined seam no longer appears irregular. Growth was continued for 44 hours total ($\sim 22\mu\text{m}$) and the joint still appeared excellent along with diamond homoepitaxial regions away from the joint.

A second and more demanding diamond/Si bonded sample was attempted; one where the gap was $\sim 50\mu\text{m}$ wide prior to growth. Since it is possible to bond diamonds much closer together than this, we consider this example nearly a "worst case" scenario for epitaxially joining diamonds. It is important to consider this possibility because one or two diamonds might get slightly misaligned when attempting to make a large-area tiled array. Again, sequential growth

runs were performed, and the sample was inspected with SEM between runs. After the first epitaxial diamond growth run of 4 hr. ($\sim 2\mu\text{m}$), this bonded pair of diamonds was found to have a topography that appears excellent near the gap and away from the gap (Fig. 7). The procedure was continued until $\sim 75\mu\text{m}$ of epitaxial diamond was grown, and the topography of the epitaxial diamond continued to appear excellent at and away from the joint after each run. A measured estimate of the rate of gap closing between the diamonds indicated that the gap closed at a rate of $\sim 0.5\mu\text{m}\cdot\text{hr}^{-1}$. This is comparable to the vertical growth rate, although since lateral epitaxial growth occurs from both diamonds, the actual lateral epitaxial growth rate appears to be approximately one half the vertical growth rate. Fig. 8 shows SEM micrographs after the final growth run. In the low magnification, angled micrograph, the stagger between the crystals can be seen, as there was no attempt to align the non-bonding edges such that they would be coplanar. The topography of the diamonds appeared smooth, although a few discrete asperities were observed on the growth face. A third attempt at epitaxially joining two diamonds that had a $10\mu\text{m}$ gap was made. It was as successful as those described above.

3. Characterization of the Epitaxially Joined Diamonds

The first two attempts at epitaxially joining diamonds bonded to Si with Ni were characterized further. The two samples were characterized somewhat differently, so it is instructive to present the results from both.

First Epitaxially Joined Sample (original gap $\sim 4\mu\text{m}$)

A stylus profilometer was used to measure the step height across the epitaxial joint. The height was measured to be $\sim 3\mu\text{m}$, which is consistent with the SEM micrographs in Fig. 6. This step is most probably due to the difference in starting thicknesses of the two diamonds used in the experiment. Nevertheless, we consider this to be excellent registry which can be attributed to the holding of a tight thickness tolerance when the vendor polished the diamond wafers ($\pm 5\mu\text{m}$). MicroRaman spectroscopy was then obtained from the sample. An Ar ion laser emitting 514.5nm wavelength light was used in conjunction with a microscope to focus the beam to $\sim 10\mu\text{m}$ spot

size. Fig. 9 shows the spectra obtained from the joint region and a region of the homoepitaxial film away from the joint for comparison. Of course, the predominant feature in both spectra is the diamond LO phonon line at 1332 cm^{-1} . Note that there is a small peak at $\sim 1470\text{ cm}^{-1}$ in the spectrum from the joint area, which is associated with sp^2 bonding. There is also broadband luminescence at increasing wave number from the joint region. A comparison of diamond LO phonon line widths was also made. The full width at half maximum (FWHM) from the joint region was 4.1 cm^{-1} , which compares favorably with a FWHM of 3.9 cm^{-1} away from the joint. Although the difference between these values is small, which is encouraging, both values are considered larger than expected for high quality homoepitaxial diamond films. This had to do with the Raman spectrometer settings which were not optimized for ultimate resolution in this case.

The sample was then loaded into our integrated processing system [26], which has facility for doing low energy electron diffraction (LEED). The LEED data verifies that (100) homoepitaxy has been achieved for both diamond crystals. The LEED spots from both crystals are sharp and clear and minimal background (or diffuse) scattering is seen. This is indicative of well-ordered, topographically excellent homoepitaxial surfaces, which is consistent with the SEM results presented earlier. The LEED was observed while the sample was translated back and forth such that each crystal was respectively being struck by the low energy electron beam. The patterns were seen to shift slightly on the screen from diamond to diamond. When the sample is positioned such that the electron beam is striking both diamonds, a double spot arrangement is observed (Fig. 10). These two coincident LEED patterns are clearly translated with respect to each other, and there is also a small rotation of the patterns with respect to each other. For the purposes of preliminary analysis, it is instructive to estimate the angles associated with the LEED pattern shift and rotation. Using the geometry of the LEED apparatus and the distance measured between the spots (pattern shift), this angle is estimated to be $\sim 3^\circ$. Measuring the rotational component directly from the pattern, we find that angle is $\sim 0.5^\circ$. We are tentatively associating these angles with a small crystallographic misorientation ($\sim 3^\circ$) between the diamonds; however, it

is recognized that if the two diamond surfaces are not parallel, this may also contribute to the LEED pattern shift that is observed. If this interpretation is correct, this would be consistent with the crystallographic tolerance held by the diamond vendor of $\{100\} \pm 2^\circ$ for all faces and edges.

Second Epitaxially Joined Sample (original gap $\sim 50\mu\text{m}$)

A stylus profilometer measurement across this epitaxial joint showed the step height to be $\sim 6\mu\text{m}$, which is consistent with the SEM micrograph in Fig. 8 and is still consistent with the diamond thickness tolerance of $\pm 5\mu\text{m}$. MicroRaman spectroscopy was again used to assess the quality of this epitaxial joint, and instrumental settings were chosen to optimize resolution while permitting a reasonable count rate. Like the first sample, the predominant feature in both spectra is the diamond LO phonon line at 1332 cm^{-1} . In the spectrum taken from the joint region there is a small peak at $\sim 1470\text{ cm}^{-1}$ (sp^2 bonding), and there is broadband luminescence observed at higher wave numbers. Essentially, the Raman spectroscopy features are very similar to those from the first sample.

A comparison of diamond LO phonon line widths and positions was also made. The peak position of the LO phonon mode can be related to the residual elastic strain in the epitaxial layer. These results are compiled in Table 2 along with microRaman spectroscopy results from a type Ia diamond which is used for comparison and calibration. What is interesting to note are the narrow line widths achieved. The joint region has a line width comparable to natural type Ia single crystal diamond, and the homoepitaxial diamond away from the joint has a FWHM that is 0.6 cm^{-1} less than both of those. Also, there is a shift of the diamond LO phonon peak position to higher vibrating frequency with respect to the natural LO phonon frequency of the type Ia single crystal diamond at 1332.0 cm^{-1} . This shift in the LO phonon mode to a higher frequency is indicative of compressive strain (or decreased lattice parameter) in the epitaxially joined region. This contrasts with no measurable shift in the LO phonon peak position from the homoepitaxial diamond grown away from the joint. Although strain-free material would be most preferable, the fact that the observed strain is compressive in nature (rather than tensile) represents the lesser threat to joint integrity via cracking. It should be noted that we have not observed any sign of cracking

anywhere in the grown homoepitaxial films - at the joint or away from the joint. Compressive strain at the epitaxial joint can be understood in the context of the difference in coefficients of thermal expansion between the Si and diamond wafers. Silicon has a higher linear coefficient of thermal expansion ($2.5 \times 10^{-6} \text{ K}^{-1}$ at 300K) than diamond ($1.1 \times 10^{-6} \text{ K}^{-1}$ at 300K). Assuming that the entire bonded structure is strain free at the growth temperature of $\sim 600^\circ\text{C}$, the thermal excursion to ambient temperature would tend to put the diamond into compression and the Si into tension. It is then reasonable to expect that the epitaxial joint, being of lesser cross section, accommodates some of this thermal strain elastically. Additional thermal strain has the potential to be accommodated elsewhere in the bonded structure, and thermal strain remains a subject of concern for scaling a bonded and epitaxially joined diamond array to larger areas.

Destructive testing was then performed to examine the epitaxial joint in more detail. The entire structure was placed in a Nitric/HF/Acetic Acid solution to etch away the Si substrate and reacted Ni-containing region. This left the two transparent diamonds still joined to each other and this entire structure was able to be handled with tweezers thereby further demonstrating that an epitaxial joint had indeed been formed and could withstand some degree of mechanical loading. The epitaxial joint was then fractured in order to examine details associated with the interior of the joint. This is shown in Fig. 11. It appears that anywhere from $\sim 30\mu\text{m}$ - $50\mu\text{m}$ of the total epitaxial thickness was actually epitaxially joined as indicated by the fracture morphology. Indeed, the epitaxial joint thickness, as measured vertically from the top of the diamond down to where fracture appears to have ceased, does vary quite a bit. This is consistent with the SEM observations after each run that often showed different regions of the overgrowing epitaxial layer to be closer to contact with the adjacent side. Also, these values of epitaxial joint thickness are roughly consistent with the fact that the lateral epitaxial growth rate is about one half that of the vertical rate with this process as described earlier. Finally, one portion of the sample (one diamond with epi and fractured seam), was then subjected to an oxidizing flame to assess the difference in defect densities by etch pit formation. This characterization technique has been used previously to delineate defects in natural single crystal diamonds, CVD polycrystalline diamond

films, and homoepitaxial diamond [20, 27]. Fig. 12 does show an increased dislocation density in the seam/joint region, which is qualitatively consistent with the somewhat broadened MicroRaman peak and the potential for a small crystallographic misorientation between the two starting diamond crystals. The defect density in the homoepitaxial region away from the joint is approximately 10^6 cm^{-2} , which has been observed in other homoepitaxial films grown in our laboratory [19, 20]. In the region extending $\sim 25\mu\text{m}$ from the fracture edge, the defect density is high enough such that the etch pits overlap each other thereby making a measurement not necessarily reliable. A lower limit for the defect density in this region is estimated to be $\sim 10^7 \text{ cm}^{-2}$. It should be pointed out that the transition between the higher defect density region of the joint and the lower defect density homoepitaxial region adjacent and away from the joint is abrupt. In other words, it appears that dislocations formed during the epitaxial joining process do not propagate beyond the dimensions of the original gap between the diamond crystals -- at least for a growth thickness of $\sim 75\mu\text{m}$. While this higher dislocation density in the joint region is not considered satisfactory, it should still be possible to reap the advantages of a large area diamond single crystal as long as the areas of high dislocation density are predictable and restricted. For example, electronic devices could be built in the vast majority of the homoepitaxial diamond not in the higher defect density joint region with proper mask set design and alignment. It also may be possible to optimize steps in the above described processes to minimize the defect density in the joint region. Future work to address this issue might include starting with diamonds that have tighter crystallographic tolerances and/or exploration of extended homoepitaxial diamond growth. In any case, thicker diamond homoepitaxial growths would need to be investigated with our process to see if a propagation or reduction of the dislocation density would be realized.

4. Summary

The development of a multi-step process to epitaxially join single crystal diamonds has been demonstrated. The deposition of epitaxial Ni on one surface of the diamonds and subsequent reaction with a Si wafer to bond them in close proximity appears to be compatible

with the water/alcohol CVD diamond deposition process developed to epitaxially join the crystals. The ability to bridge (or close) gaps between diamond crystals of up to $\sim 50\mu\text{m}$ has been shown, which represented a "worst case" scenario. If the diamonds are positioned correctly upon bonding to the Si wafer, these gap distances have been and can be very much reduced, thereby reducing the time to epitaxially overgrow and join diamonds. Subsequent characterization of epitaxially joined diamonds has shown the joint to be robust and to be of reasonable quality considering the slight (and expected) crystallographic misorientation of the crystals. Further development of steps in this process could potentially lead to lower defect densities in the joint region. In conclusion, it appears that this demonstration of epitaxial joining of two diamond single crystals justifies the scaling up of this process to an array of diamonds in order to fabricate a large-area single crystal diamond substrate.

Acknowledgments

We wish to thank G.G. Fountain (RTI), P. Ingram (RTI), and R. Kessler (Univ. of North Carolina - Chapel Hill) for their scientific expertise and helpful discussions. The authors gratefully acknowledge support of this work by BMDO/IST through the Office of Naval Research (Contract No. N00014-92-C-0081).

References

- [1] J.E. Field, Editor: The Properties of Natural and Synthetic Diamond (Academic Press, London, 1992).
- [2] M. Seal, Proc. 1st Intl. Conf. Applications of Diamond Films and Related Materials - ADC '91, Eds. Y. Tzeng, et al. (Elsevier, 1991) 3 and many other manuscripts in this proceedings.
- [3] M.N. Yoder, Proc. 1st Intl. Conf. Applications of Diamond Films and Related Materials - ADC '91, Eds. Y. Tzeng, et al. (Elsevier, 1991) 287.
- [4] A. J. Tessmer, K. Das, and D.L. Dreifus, Diamond and Related Materials, 1 (1992) 89.
- [5] L.M. Edwards and J.L. Davidson, Diamond and Related Materials, 2 (1993) 808.

- [6] S. Koizumi, T. Murakami, T. Inuzuka, and K. Suzuki, *Appl. Phys. Lett.*, 57 (1990) 563.
- [7] L. Wang, P. Pirouz, A. Argoitia, J.S. Ma, and J.C. Angus, *Appl. Phys. Lett.*, 63 (1993) 1336.
- [8] A. Argoitia, J.C. Angus, L. Wang, X.I. Ning, and P. Pirouz, *J. Appl. Phys.*, 73 (1993) 4305.
- [9] W. Zhu, P.C. Yang, and J.T. Glass, *Appl. Phys. Lett.*, 63 (1993) 1640.
- [10] B.R. Stoner and J.T. Glass, *Appl. Phys. Lett.*, 60 (1992) 698.
- [11] X. Jiang, C.-P. Klages, R. Zachai, M. Hartweg, and H.-J. Fusser, *Appl. Phys. Lett.*, 62 (1993) 3438.
- [12] R.A. Rudder, J.B. Posthill, G.C. Hudson, D.P. Malta, R.E. Thomas, R.J. Markunas, T.P. Humphreys, and R.J. Nemanich, *Proc. 2nd Intl. Conf. New Diamond Science and Technology, 1991 MRS Int. Conf. Proc.* (1991) 425.
- [13] M.W. Geis, H.I. Smith, A. Argoita, J. Angus, G.-H.M. Ma, J.T. Glass, J. Butler, C.J. Robinson, and R. Pryor, *Appl. Phys. Lett.*, 58 (1991) 2485.
- [14] G. Janssen and L.J. Giling, *Diamond and Related Materials, Diamond Films '94, (Il Ciocco, Italy, 1994) in press.*
- [15] G. Janssen and L.J. Giling, *Proc. 4th Intl. Conf. New Diamond Science and Technology, Eds. S. Saito, et al., (Kobe, Japan, 18-22 July 1994) 295.*
- [16] J.B. Posthill, R.A. Rudder, G.C. Hudson, D.P. Malta, G.G. Fountain, R.E. Thomas, R.J. Markunas, T.P. Humphreys, R.J. Nemanich, and D.R. Black, *Proc. 2nd Intl. Symp. Diamond Materials, 91-8 [The Electrochemical Society] (1991) 274.*
- [17] Vendor for polished and oriented diamond single crystals: Harris Diamond Corp., Mount Arlington, New Jersey, USA; distributor for: Drukker International, Cuijick, The Netherlands.
- [18] R.A. Rudder, G.C. Hudson, J.B. Posthill, R.E. Thomas, R.C. Hendry, D.P. Malta, R.J. Markunas, T.P. Humphreys, and R.J. Nemanich, *Appl. Phys. Lett.*, 60 (1992) 329.
- [19] J.B. Posthill, T. George, D.P. Malta, T.P. Humphreys, R.A. Rudder, G.C. Hudson, R.E. Thomas, and R.J. Markunas, *Proc. 51st Ann. Meeting Microsc. Soc. of America, G.W. Bailey and C.L. Rieder, Eds. (San Francisco Press, 1993) 1196.*

- [20] J.B. Posthill, D.P. Malta, G.C. Hudson, T.P. Humphreys, R.A. Rudder, R.E. Thomas, and R.J. Markunas, unpublished research (1994-1995).
- [21] T.P. Humphreys, H. Jeon, R.J. Nemanich, J.B. Posthill, R.A. Rudder, D.P. Malta, G.C. Hudson, R.J. Markunas, J.D. Hunn, and N.R. Parikh, *Mater. Res. Soc. Symp. Proc.*, 202 (1991) 463.
- [22] M.F. Singleton and P. Nash, C-Ni Phase Diagram in: *Binary Alloy Phase Diagrams*, Vol. 1, Eds. T.B. Massalski, et al. (American Society for Metals, Metals Park, 1986) 578.
- [23] Vendor for polished and oriented Ni(100) crystals: Monocrystals Co., Cleveland, Ohio, USA.
- [24] G.G. Fountain, S.V. Hattangady, R.A. Rudder, J.B. Posthill, and R.J. Markunas, *Mater. Res. Soc. Symp. Proc.*, 146 (1989) 139.
- [25] R.A. Rudder, J.B. Posthill, G.C. Hudson, M.J. Mantini, and R.J. Markunas, *Diamond Optics*, SPIE, 969 (1989) 72; and unpublished work in this laboratory (1994).
- [26] R.A. Rudder, R.C. Hendry, and R.J. Markunas, *J. Vac. Sci. Technol. A*, 7 (1989) 802.
- [27] D.P. Malta, J.B. Posthill, R.A. Rudder, G.C. Hudson, and R.J. Markunas, *J. Mater. Res.*, 8 (1993) 1217.

Tables

TABLE 1: Electron microprobe measurements of concentration in atomic percent (carbon determined by subtraction). Accuracy is only $\sim \pm 10\%$ relative due to surface roughness of cleaved cross section.

| Region | C | Si | Ni | Si:Ni Atomic Ratio |
|-------------|------|------|------|--------------------|
| Upper Layer | 47.2 | 22.1 | 30.7 | 0.72 |
| Lower Layer | 40.2 | 37.4 | 22.4 | 1.67 |

TABLE 2: MicroRaman spectroscopy results from the second epitaxially joined diamond sample and natural, type Ia (100) diamond.

| Region | LO Phonon | LO Phonon | LO Phonon |
|--------------------|-----------------------------------|--------------------------------|--------------------------|
| | Peak Position (cm ⁻¹) | Peak Shift (cm ⁻¹) | FWHM (cm ⁻¹) |
| Type Ia (standard) | 1332.0 | 0.0 | 3.0 |
| At Joint | 1332.3 | +0.3 | 3.0 |
| Away from Joint | 1332.0 | 0.0 | 2.4 |

Figure Captions

Fig. 1 Characterization of MBE-grown heteroepitaxial Ni on C(100); (a) SEM micrograph showing relatively smooth topography, and (b) RBS/channeling spectrum verifying (100) Ni epitaxy and reasonable Ni crystal quality ($\chi_{\min} \cong 3\%$ and $\chi_{\text{int}} \cong 15\%$). Thickness of Ni film is $\sim 128\text{nm}$.

Fig. 2 SEM micrographs showing two edge-oriented and Ni-coated diamonds that were bonded to a Ni(100) crystal; (a) both diamonds are shown after bonding at low magnification, (b) a perspective view of the edges of both diamonds showing the gap and deformation of the underlying Ni crystal, and (c) a $10\mu\text{m}$ separation was observed between the bonded diamonds.

Fig. 3 Low and higher magnification micrographs showing a tiled array consisting of four diamonds that were bonded to a Si wafer via Ni/Au/W/SiO₂ interlayers. The entire array is shown in (a). The background contrast observed in this optical micrograph is due to the reacted Ni and Au at the bonded (underside) interface. The edges were as close as $\sim 1.5\mu\text{m}$ in regions as seen in (b) via SEM.

Fig. 4 Schematic diagram showing the bonding of two Ni-coated diamonds in close proximity to each other on a Si wafer.

Fig. 5 SEM examination of details of Ni-coated diamonds bonded to Si wafers; (a) fracture surface that remained on the Si wafer after bonding and intentionally prying the diamond off. Note the featureless "cross" which is where Ni was not deposited on the diamond and hence no diamond/Si bonding occurred. Cleaved cross section of another diamond/Si bonded sample is shown in (b) with the reacted region labeled as "Ni(100)".

Fig. 6 SEM micrographs from the first sample showing topography of gap/joint region and a homoepitaxial region away from gap/joint. After first growth run of 4 hr. ($\sim 2\mu\text{m}$); (a) gap and (b) away from gap region. After fourth growth run - 16 hr. total ($\sim 8\mu\text{m}$) the diamond have been joined epitaxially; (c) joint region showing step and (d) away from joint region. After eleven growth runs - 44 hr. total ($\sim 22\mu\text{m}$) the joint region and away from the joint topographies appear good; (e) joint region showing step and (f) away from joint region.

Fig. 7 SEM micrographs from the second sample after the first diamond growth run of 4 hr. ($\sim 2\mu\text{m}$) showing; (a) the gap of $\sim 50\mu\text{m}$, and (b) excellent homoepitaxial topography away from the gap.

Fig. 8 SEM micrographs from the second epitaxially joined sample after $\sim 75\mu\text{m}$ of homoepitaxial diamond growth; (a) low magnification perspective view of joint region and sides of the two diamond crystals, (b) higher magnification of the step observed at the joint, and (c) excellent topography away from the joint.

Fig. 9 MicroRaman spectra from the first epitaxially joined sample taken from; (a) the joint region, and (b) away from the joint.

Fig. 10 LEED pattern from the first epitaxially joined sample. The electron beam is striking both diamond crystals, and two translated and rotated patterns are observed.

Fig. 11 SEM micrographs from the fractured epitaxial joint region. A perspective view showing the side of a diamond that was adjacent to the other diamond with the fractured region at the top is seen in (a), while an edge-on view of the fracture is observed in (b).

Fig. 12 SEM micrographs from a bonded and joined diamond after fracture and exposure to an oxidizing flame for 2 sec. A perspective view is shown in (a) with the fractured joint at the front, while a plan-view perspective is shown in (b) with the fractured epitaxial joint at the left. The etch pit density is observed to decrease abruptly $\sim 25\mu\text{m}$ from the fracture edge.

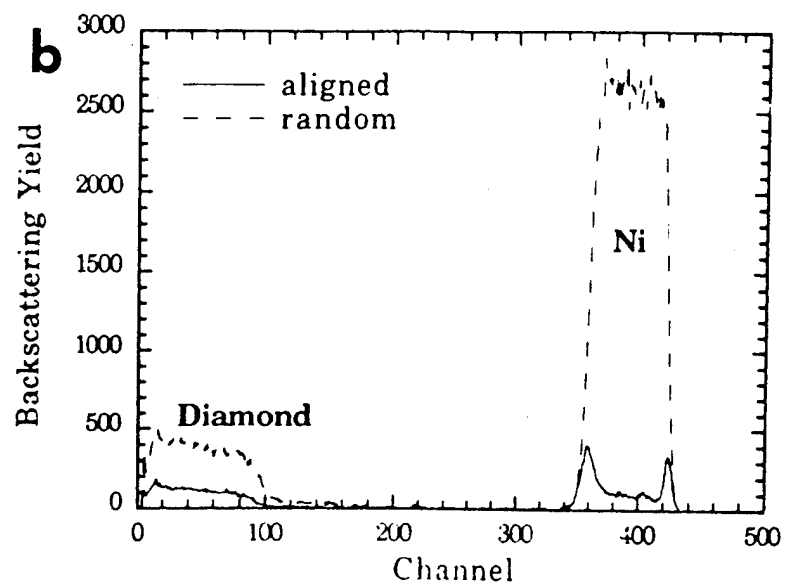
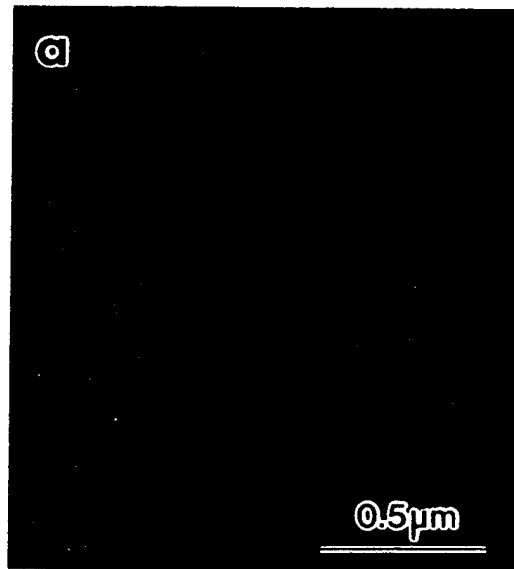


Fig. 1

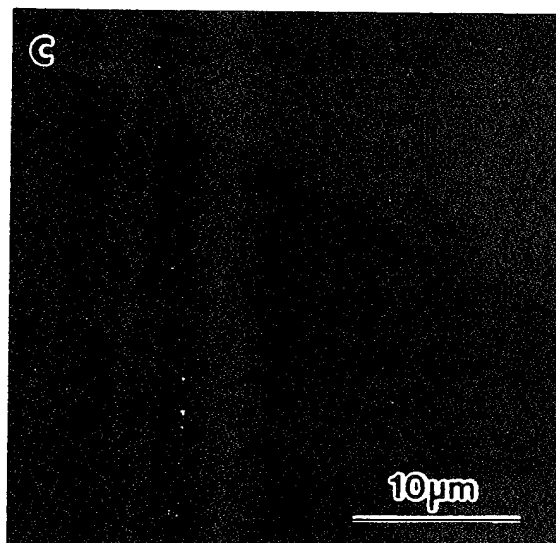
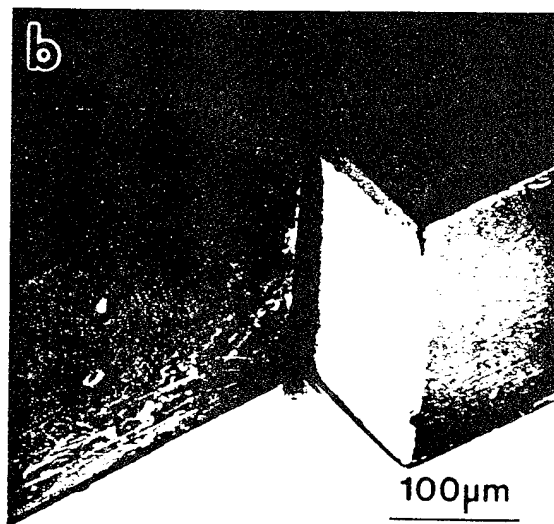
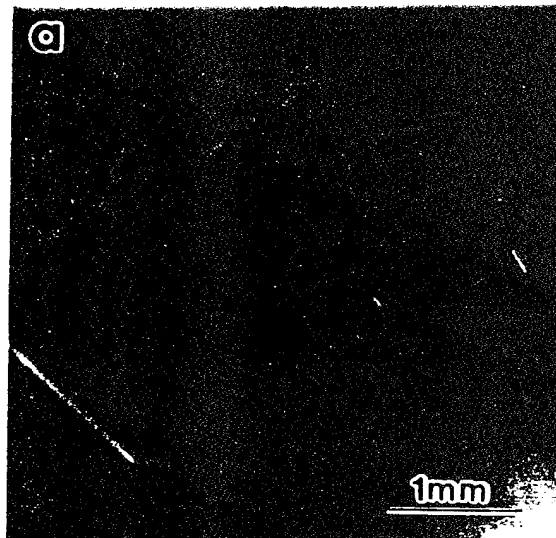


Fig. 2

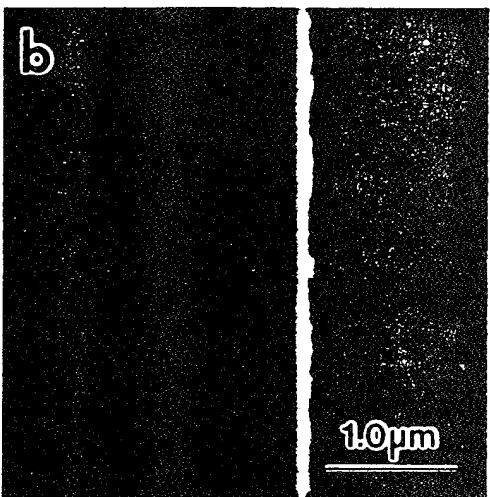
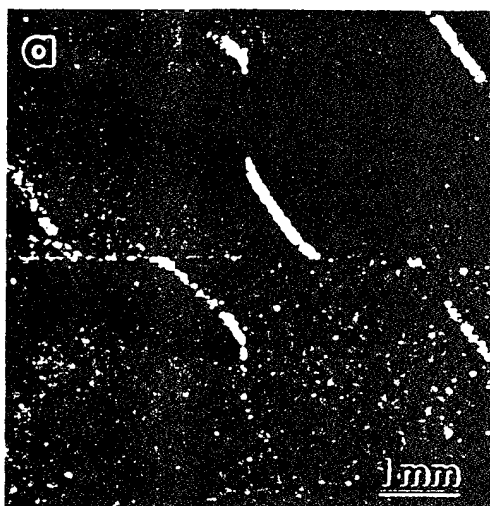


Fig. #3

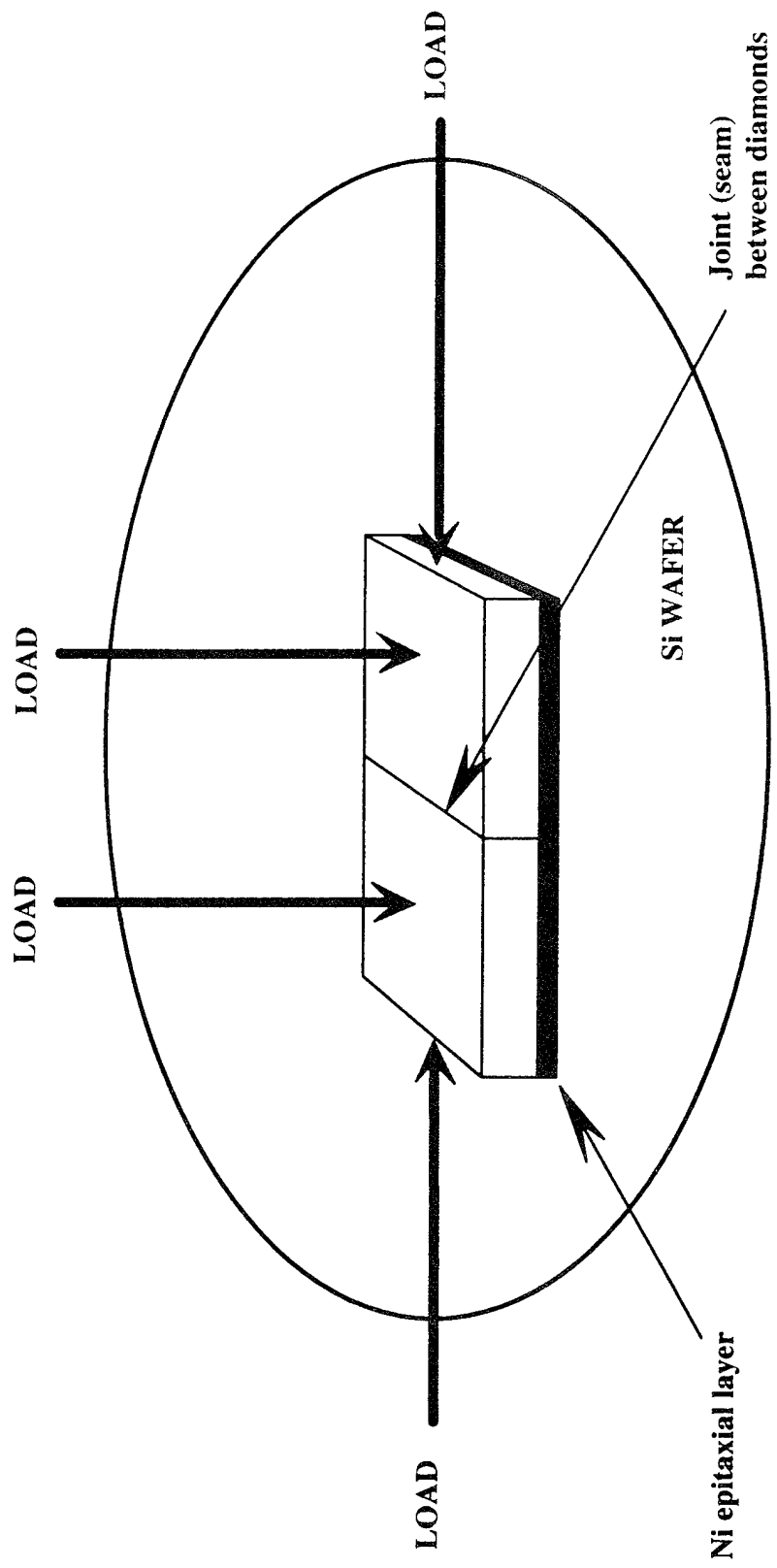


Fig. 4

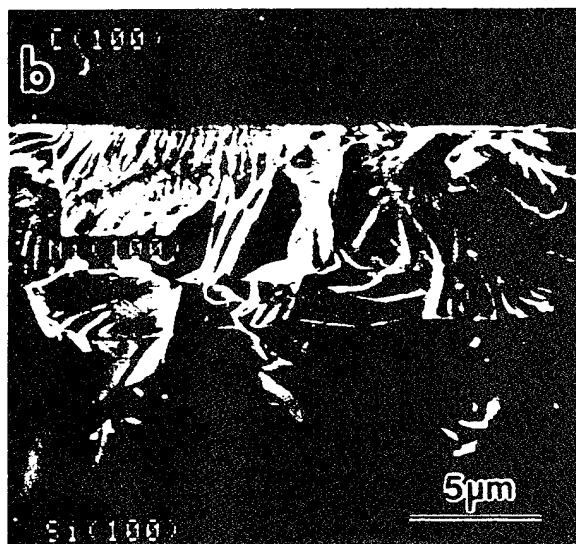
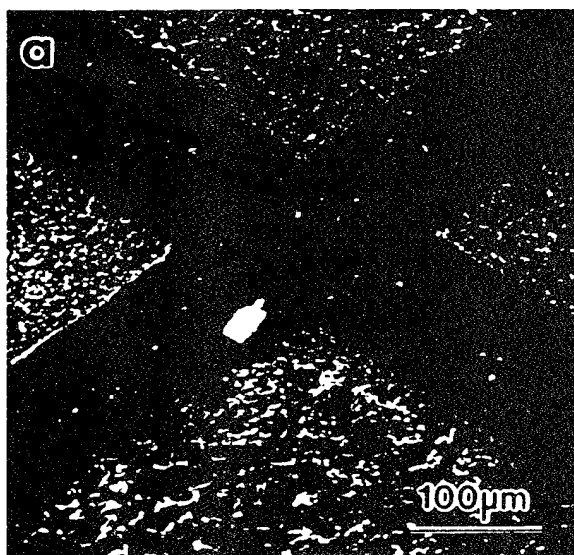


Fig. 5

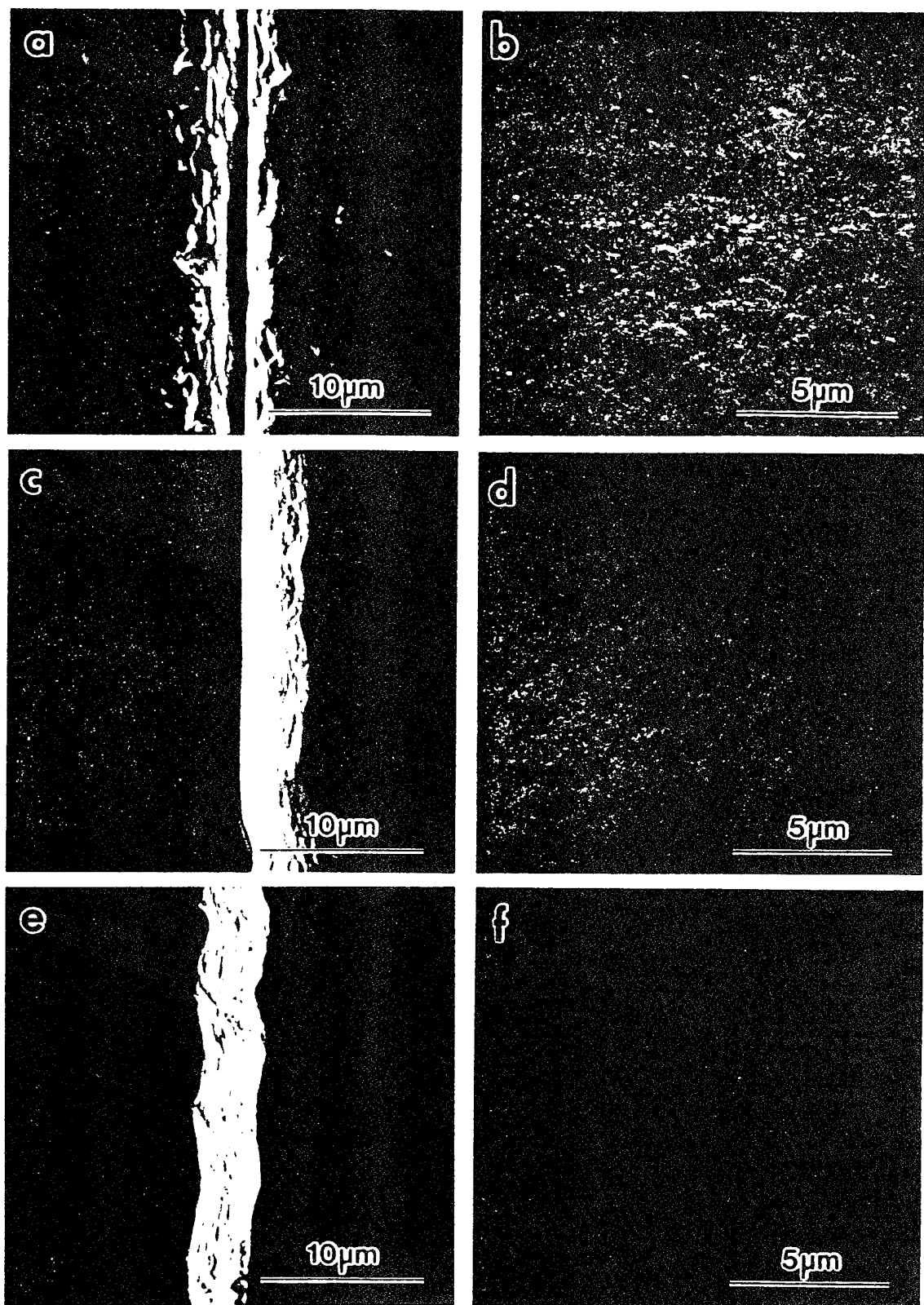


Fig. 6

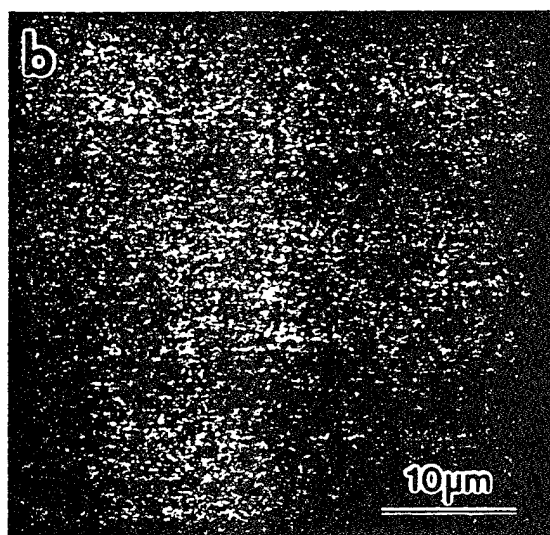
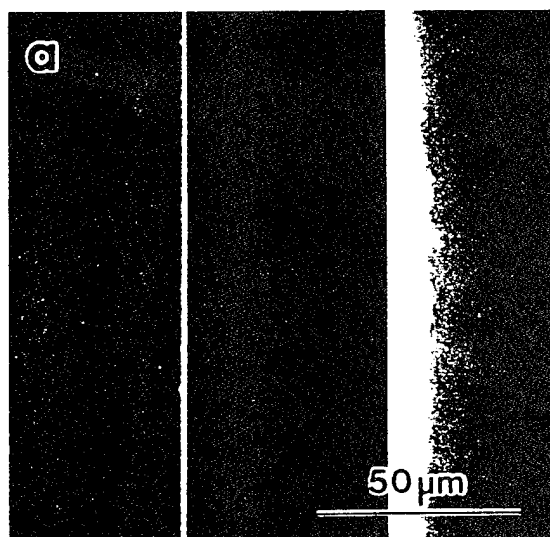


Fig. 7

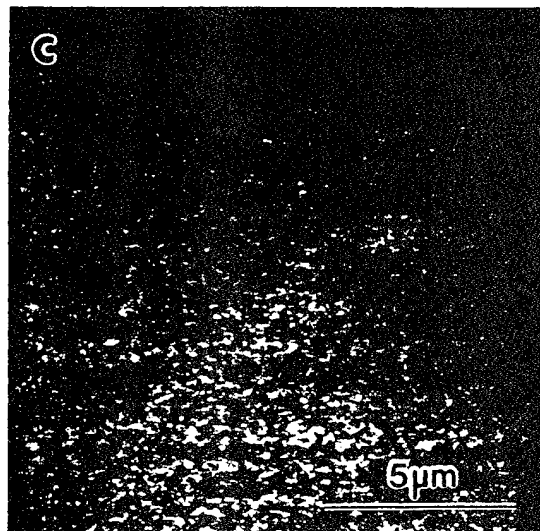
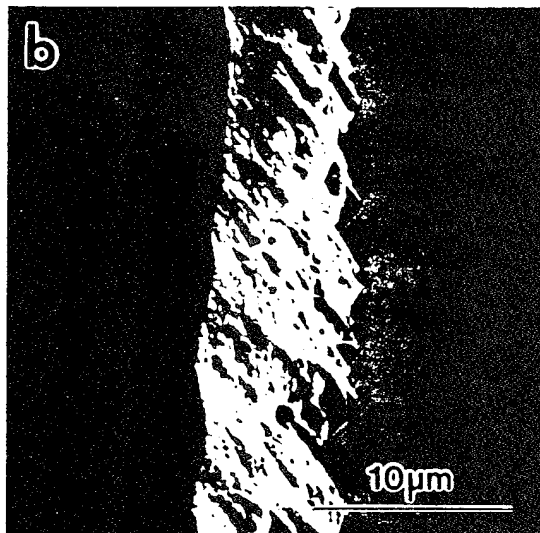
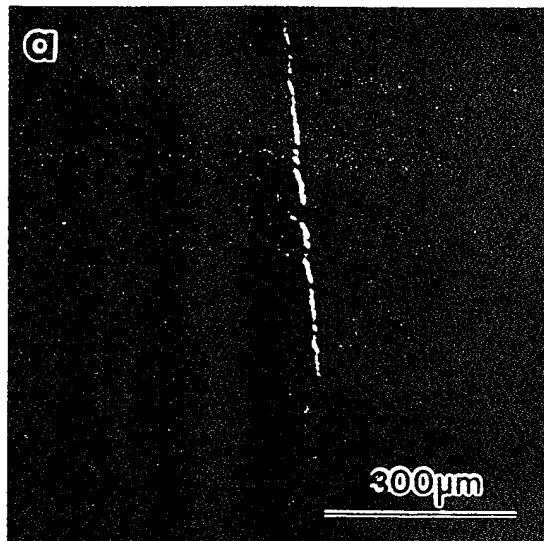


Fig. 8

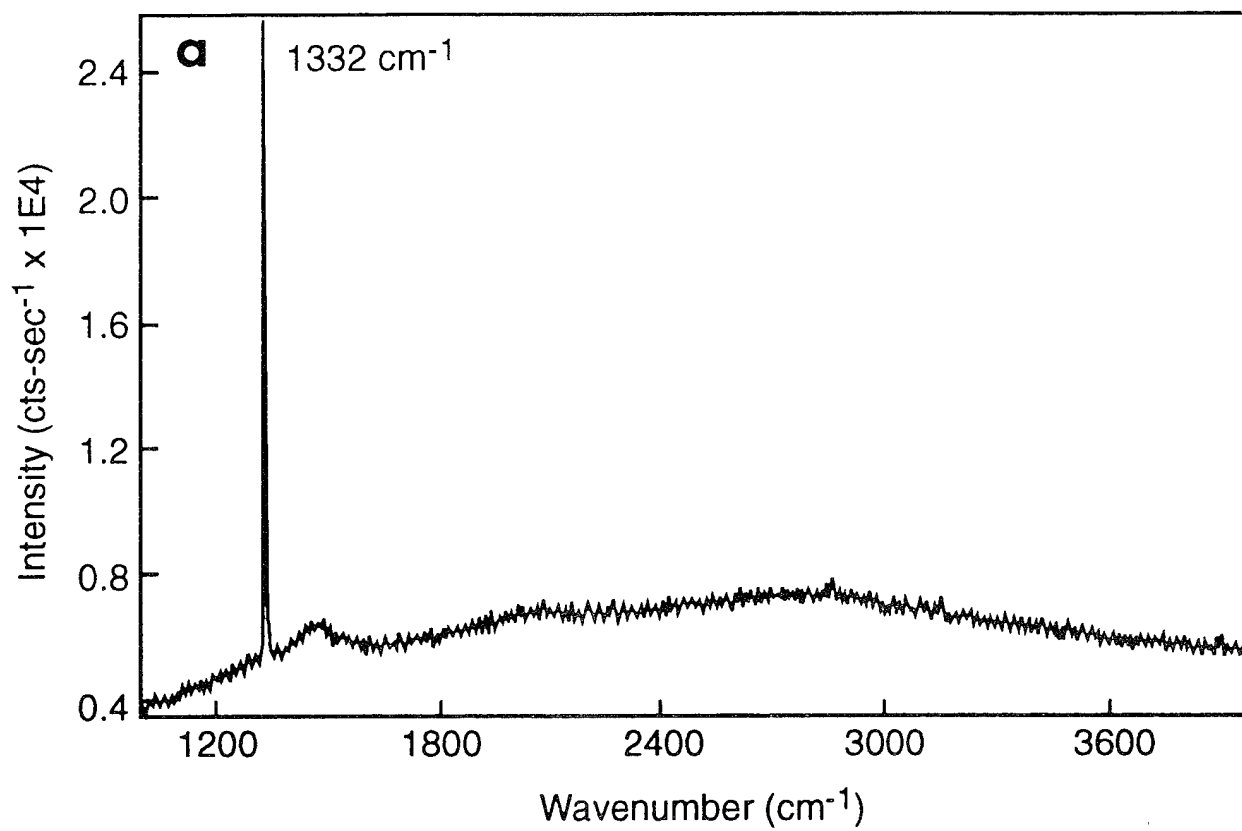


Fig. ~~Ha~~ 9a

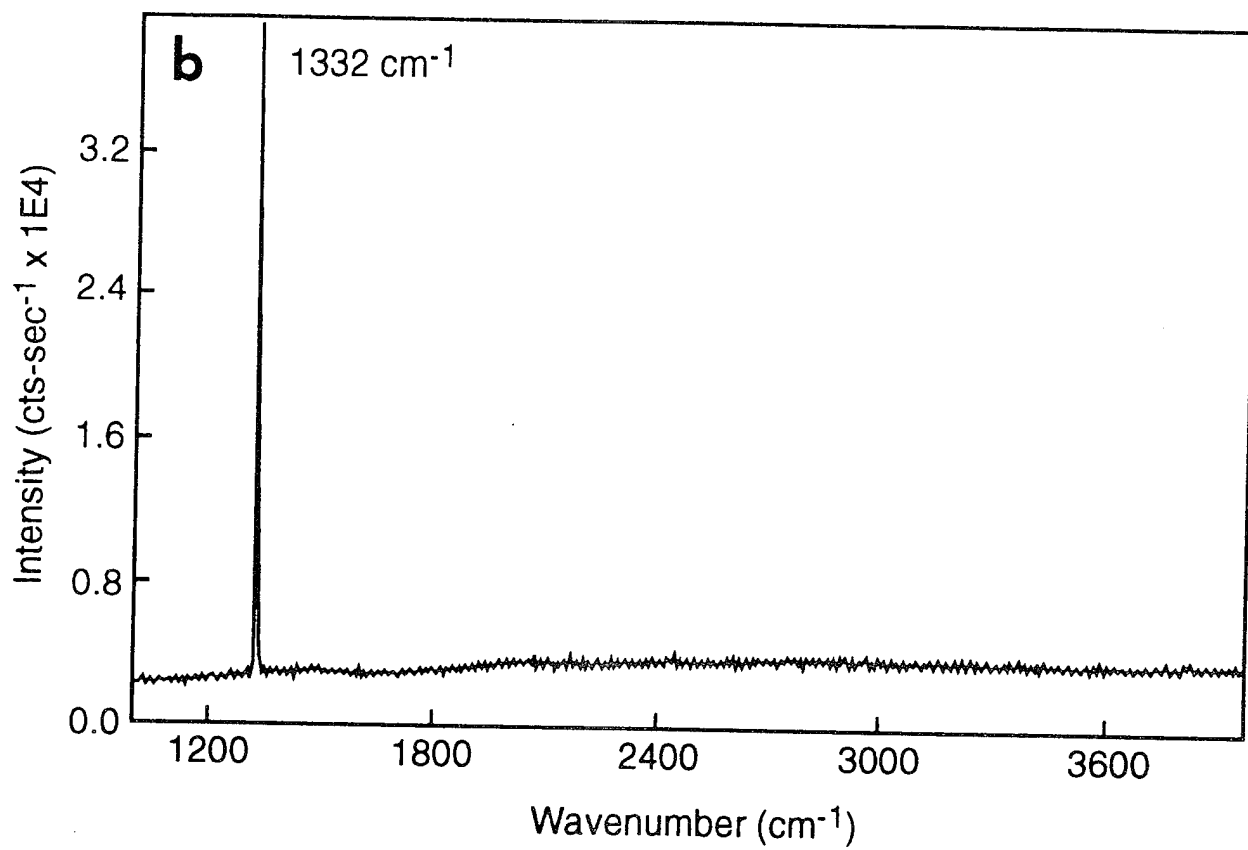


Fig. ~~116~~ 96

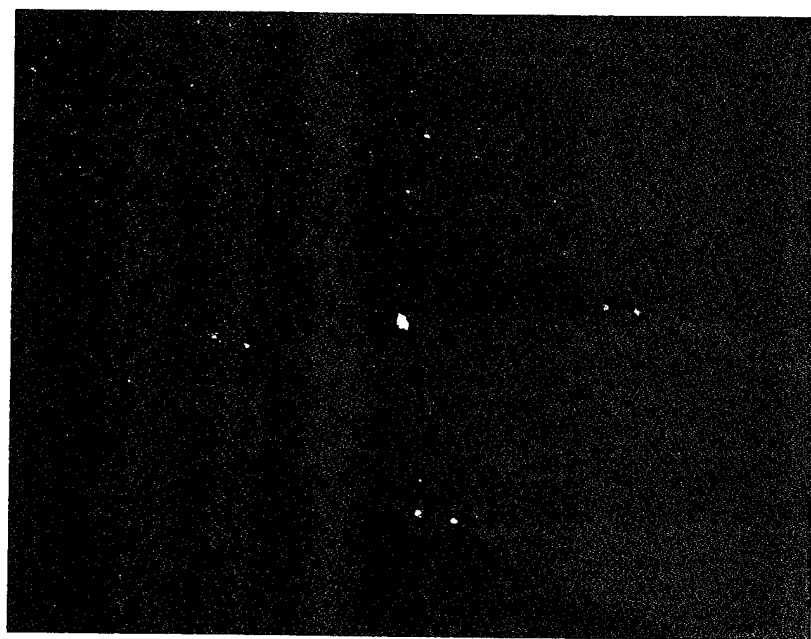
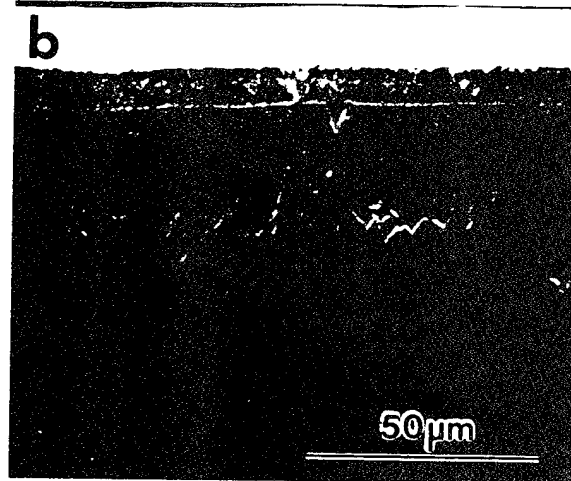
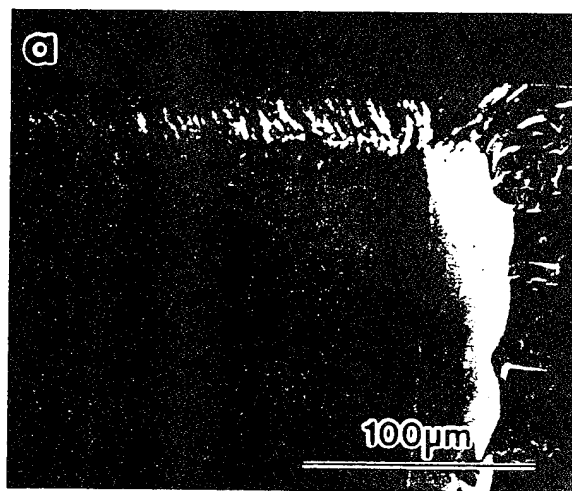


Fig. ~~12~~ 10



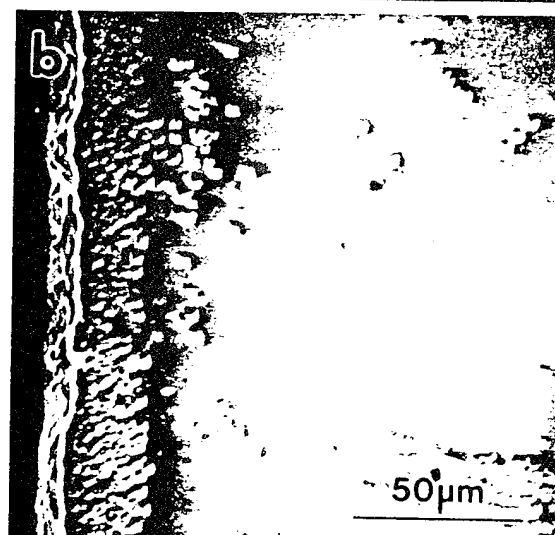
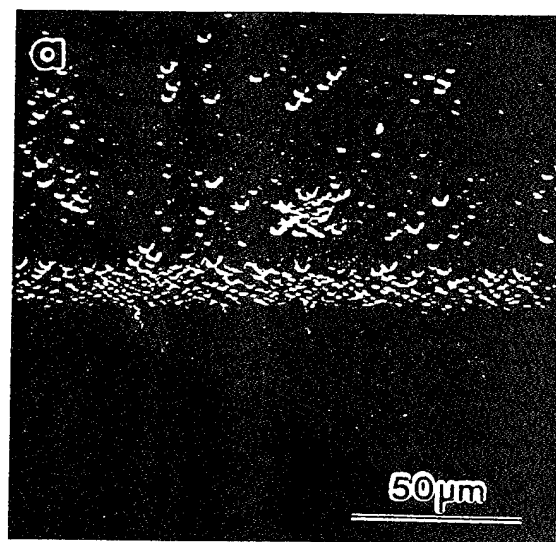


Fig. ~~15~~ 12

PROCESS OF EPITAXIAL JOINING TO FABRICATE A LARGE-AREA DIAMOND SINGLE CRYSTAL

D.P. Malta, J.B. Posthill, G.C. Hudson, R.E. Thomas,
T.P. Humphreys, R.A. Rudder, and R.J. Markunas
Research Triangle Institute
Research Triangle Park, NC 27709-2194

We have demonstrated the fabrication of a large-area diamond single crystal using a multi-step epitaxial joining process. In this process, 3mm×3mm square C(100) crystals were successfully bonded to a Si substrate in close proximity to each other. The diamonds were then joined into a single crystal plate via epitaxial layer overgrowth. Surface topography was excellent. MicroRaman spectroscopy showed the LO phonon mode line at 1332cm⁻¹ with a FWHM of 3.0cm⁻¹ and 2.4cm⁻¹ measured at and away from the joint, respectively. Examination of the fractured joint revealed a thickness of 30-50μm indicating that the lateral rate of gap closure and the vertical growth rate were of the same order making this a reasonably efficient process. A higher defect density was observed at the joint but it was contained to the dimension of the original gap between the crystals (~50μm). Our results indicate that this epitaxial joining process can be scaled to a larger array in order to obtain a diamond single crystal of desired area.

INTRODUCTION

The realization of a viable diamond-based electronics technology requires the availability of large-area diamond single crystals. The limited supply and prohibitive cost of large, high crystalline quality natural diamond crystals makes their use in electronics production impractical. Nevertheless, the desire to exploit the physical properties of diamond for electronics applications has spurred a large effort to produce high quality diamond single crystal material synthetically. Although this effort has met limited success, some significant progress has been made toward the end goal. For example, highly oriented diamond films have been grown by microwave plasma chemical vapor deposition (CVD) on Si, SiC and Ni substrates (e.g. 1). Electrical properties of the highly oriented diamond films grown on Si were comparable to homoepitaxial diamond films but inferior to those of natural diamond (2) and electrical properties of polycrystalline diamond films were inferior to both (3). Heteroepitaxial diamond growth has been achieved on limited areas of small (100μm-300μm) c-BN (4) and BeO crystals (5).

An alternative approach to creating a large-area single crystal diamond is that of epitaxial joining. In this process, two or more natural diamond single crystals are arranged in close proximity to one another. A homoepitaxial diamond layer is then grown over the crystals and bridges the gap that separates them thus forming one continuous diamond crystal. Some success has already been achieved in this area. For example, Geis, et al., (6) have created patterned Si wafers with regular arrays of {111}-faceted pyramidal pits in which similarly-faceted diamond crystals were held. Growth of homoepitaxial diamond on each of the seed crystals eventually extended laterally to form a mosaic diamond film of

large area. Janssen and Giling (7) have used the epitaxial joining process to join two 2mm \times 2mm diamond crystals with faces and edges oriented to (100). The two crystals were soldered in close proximity to each other onto a Mo substrate. A homoepitaxial diamond layer was grown on them by hot-filament CVD joining them into a single crystal.

In this work, we have demonstrated epitaxial joining of single crystal diamonds with the growth of a high quality epitaxial diamond film grown by rf-plasma-enhanced CVD. We believe that this process has the potential to form the basis of a diamond boule technology in which diamond wafers may be cut from a large-area single crystal boule grown from an array of epitaxially joined seed crystals. Issues that we have addressed in developing this process include: procuring single crystal substrates that can be crystallographically oriented with respect to each other and that are compatible with good quality homoepitaxial growth, establishing a reliable homoepitaxial growth process, choosing a base-substrate, developing a method to bond the diamonds to it, and assuring that the bonding technology was compatible with the homoepitaxial diamond CVD process.

EXPERIMENTAL

The type of diamond chosen for the process was type Ia natural diamond. We have found this type of diamond to contain a lower dislocation density than type II diamonds. Despite a high density of nitrogen platelets in type Ia diamond, good quality epitaxial films have been achieved (8). In order to crystallographically orient the diamonds with respect to one another, all edges were cut and polished on the {010} planes and the top and bottom faces on (100) by a commercial vendor (9). The diamond wafer dimensions were 3.0mm \times 3.0mm \times 0.250mm. Si was chosen as the base substrate and Ni as the bonding medium since Ni readily reacts with Si to form a silicide, sticks reasonably well to diamond, and can also be grown epitaxially on diamond. Furthermore, it was found that the small amount of Ni that was exposed to the subsequent CVD diamond process did not negatively affect the diamond growth quality.

Bonding of Diamonds to Si

Ni was grown heteroepitaxially to a thickness of 2 μ m on a single (100) face of each of two 3mm \times 3mm type Ia diamonds by molecular beam epitaxy (MBE). Prior to growth, the diamonds were solvent cleaned followed by a 1min hydrogen plasma clean and in-vacuo transfer to the MBE. Epitaxial growth was performed at a substrate temperature of 300°C using solid-source electron-beam evaporation of Ni. Epitaxy was confirmed by low energy electron diffraction (LEED). The diamonds were placed Ni-side-down on the Si(100) base substrate and placed in a specially designed fixture that applies both compressive and longitudinal forces on the diamonds (Fig. 1). The fixture was then loaded into a vacuum furnace with flowing Ar and the temperature was raised to \sim 850°C. Once the temperature was reached, the heat was shut off and the fixture was allowed to cool. The process resulted in bonding of the diamonds to the Si substrate with a separation gap between diamonds of \sim 50 μ m. Other attempts have yielded bonded diamonds as close as 2 μ m apart.

Epitaxial Joining

The two diamonds, now bonded to a Si(100) substrate and positioned \sim 50 μ m apart, were next subject to immersion in ethyl alcohol and cleaned with a cotton swab to

rid the surface of particles. They were loaded into an rf-plasma-enhanced CVD chamber for diamond growth. Diamond growth was achieved using a water-alcohol process that was developed in our laboratory (10). Conditions used for this growth were: reactant flow-18 sccm ethanol and 12 sccm water; pressure = 1Torr; power (rf) = 1.5kW; growth temperature $\approx 600^{\circ}\text{C}$; growth rate $\approx 0.5 \mu\text{m/hr}$. Growths were performed for periods of several hours with interruptions to periodically inspect the quality of the film and the progress of epitaxial joining.

RESULTS

After the first growth period of 4 hours, the diamonds were removed and inspected by scanning electron microscopy (SEM). The gap has closed by about $2\mu\text{m}$ due to lateral overgrowth (Fig. 2a). The topography of the epitaxial diamond film was excellent (Fig. 2b). Diamond growth was continued with periodic inspections until $75\mu\text{m}$ of diamond was grown which was more than sufficient to bridge the gap between the two diamonds (Fig. 3a). The rate of gap closure was measured at about $0.5\mu\text{m/hr}$. This rate is comparable to the vertical growth rate, however, since the lateral epitaxial growth occurs from both sides, the rate of lateral epitaxy appears to be about one half the rate of vertical epitaxy. The vertical step height at the joint was measured to be $\sim 6 \mu\text{m}$ using a stylus profilometer and the SEM (Fig. 3b).

MicroRaman spectroscopy was used to assess the quality of the epitaxial joint. The LO phonon mode line at 1332 cm^{-1} with a FWHM of 3.0 cm^{-1} was measured at the joint and is comparable to the FWHM measured from a type Ia natural diamond. A FWHM of 2.4 cm^{-1} was measured away from the joint which was $\sim 0.6 \text{ cm}^{-1}$ less than both of those. This qualitatively indicates that the joint region has not been grown to the same perfection as away from the joint, but both regions are of reasonable crystalline quality. A shift in the diamond LO phonon peak position to higher vibrating frequency measured at the joint relative to that measured from the type Ia natural diamond standard indicates that residual compressive strain exists in the joint region. No peak shift was observed away from the joint region. The compressive strain is likely due to the difference in thermal expansion coefficients between diamond and Si, with Si having the greater expansion range such that on cooling the diamond joint would experience compression.

The Si base substrate was then etched away leaving only the free-standing epitaxially joined diamond plate. What was once two $3\text{mm}\times 3\text{mm}$ diamond crystals, now was a single $6\text{mm}\times 3\text{mm}$ diamond crystal rigid enough to be handled with tweezers. The plate was then fractured at the joint to examine the joint in cross-section. The thickness of the joint was $30\mu\text{m}$ - $50\mu\text{m}$. One half of the structure was then exposed to an oxidizing flame to assess defect density through etch pit formation (11). An increased defect density was observed in the seam/joint region, which is qualitatively consistent with the somewhat broadened microRaman peak and the potential for a small crystallographic misorientation between the two starting diamond crystals. The defect density away from the joint was approximately 10^6cm^{-2} , which is a typical density observed in other homoepitaxial layers grown in our laboratory. The pit density in the joint region was sufficiently high so that the pits overlapped making a density estimate imprecise. The lower limit of the defect density in the joint region was 10^7cm^{-2} .

DISCUSSION AND SUMMARY

Of particular importance is the fact that the higher defect density region was approximately the same dimensions as the original starting gap and was located in a predictable spot. We believe that this does not pose a problem for device structures built on such material as these higher defect regions can be avoided with an appropriate mask set.

In summary, we have developed a multistep process for the fabrication of a large-area diamond single crystal. The process uses the principle of lateral epitaxial overgrowth to join two or more smaller crystals into one larger one. Several key steps in the process have been successfully demonstrated such as alignment of the diamonds crystallographically and in close proximity to one another, bonding the diamonds to a Si substrate using an epitaxial Ni bonding medium, and development of a high quality homoepitaxial diamond growth process for epitaxial joining. The resulting homoepitaxial layer was of excellent quality. Although the joint region appeared somewhat more defective, it is believed that the quality can be improved with further process development such as better crystallographic alignment between crystals. Furthermore, the results of this epitaxial joining process appear to justify the scaling-up of this process to include an array of crystals for the fabrication of a much larger single crystal diamond plate.

ACKNOWLEDGMENTS

The authors gratefully acknowledge the support of this work by BMDO/IST through ONR (Contract No. N00014-92-C-0081).

REFERENCES

1. B.R. Stoner and J.T. Glass, Appl. Phys. Lett., **60**, 698 (1992).
2. B.R. Stoner, Chien-teh Kao, D.M. Malta, R.C. Glass, Appl. Phys. Lett., **62**, 2347 (1993).
3. D.M. Malta, J.A. von Windheim, H.A. Wynands, and B.A. Fox, J. Appl. Phys., **77**, 1536 (1995).
4. S. Koizumi, T. Murakami, T. Inuzuka, and K. Suzuki, Appl. Phys. Lett., **57**, 563 (1990).
5. A. Argoitia, J.C. Angus, L. Wang, X.I. Ning, and P. Pirouz, J. Appl. Phys., **73**, 4305 (1993).
6. M.W. Geis, H.I. Smith, A. Argoita, J. Angus, G.-H.M. Ma, J.T. Glass, J. Butler, C.J. Robinson, and R. Pryor, Appl. Phys. Lett., **58**, 2485 (1991).
7. G. Janssen and L.J. Giling, Diamond and Related Materials, Diamond Films '94, (Il Ciocco, Italy, 1994) in press.

8. J.B. Posthill, R.A. Rudder, G.C. Hudson, D.P. Malta, G.G. Fountain, R.E. Thomas, R.J. Markunas, T.P. Humphreys, R.J. Nemanich, and D.R. Black, *Proc. 2nd Intl. Symp. Diamond Materials*, 91-8 [The Electrochemical Society] (1991) 274.
9. Vendor for polished and oriented diamond single crystals: Harris Diamond Corp., Mount Arlington, New Jersey, U.S.A.; distributor for: Drukker International, Cuijck, The Netherlands.
10. R.A. Rudder, G.C. Hudson, J.B. Posthill, R.E. Thomas, R.C. Hendry, D.P. Malta, R.J. Markunas, T.P. Humphreys, and R.J. Nemanich, *Appl. Phys. Lett.*, **60**, 329 (1992).
11. D.P. Malta, J.B. Posthill, R.A. Rudder, G.C. Hudson, and R.J. Markunas, *J. Mater. Res.*, **8** 1217 (1993).

FIGURES

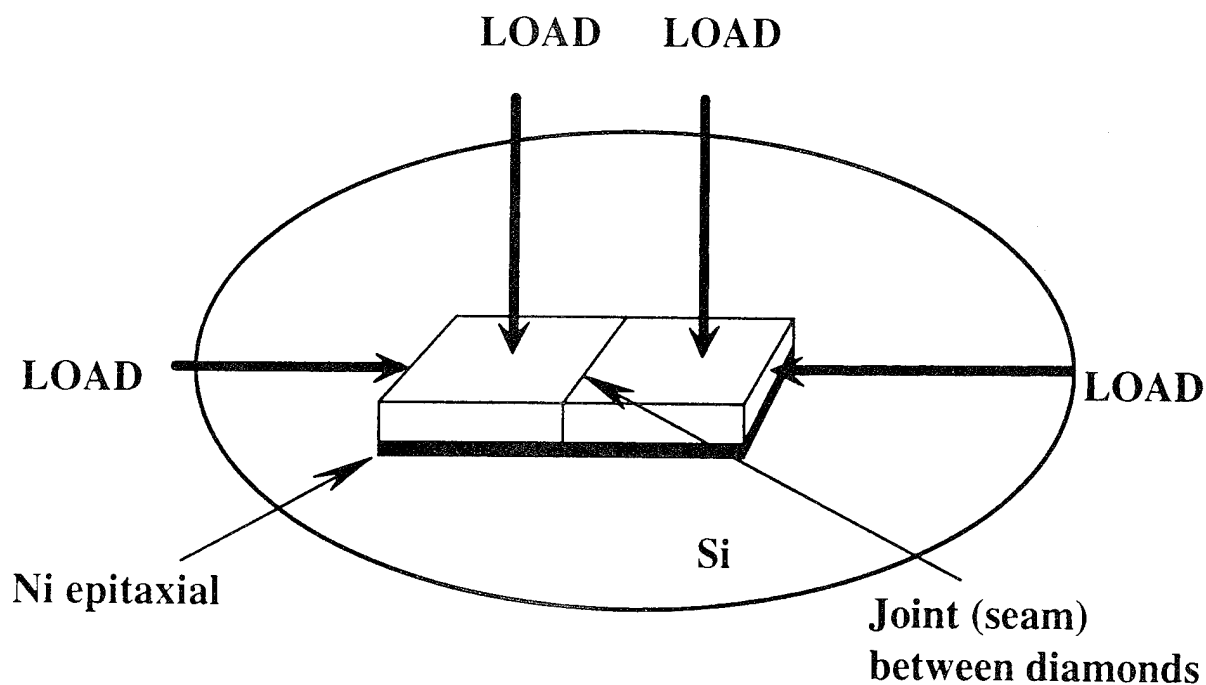


Fig.1 Schematic illustration of the bonding arrangement. The two natural diamonds are placed in close proximity to each other and loaded both vertically and longitudinally. The bond is made to the Si wafer via silicidation of the Ni bonding medium.

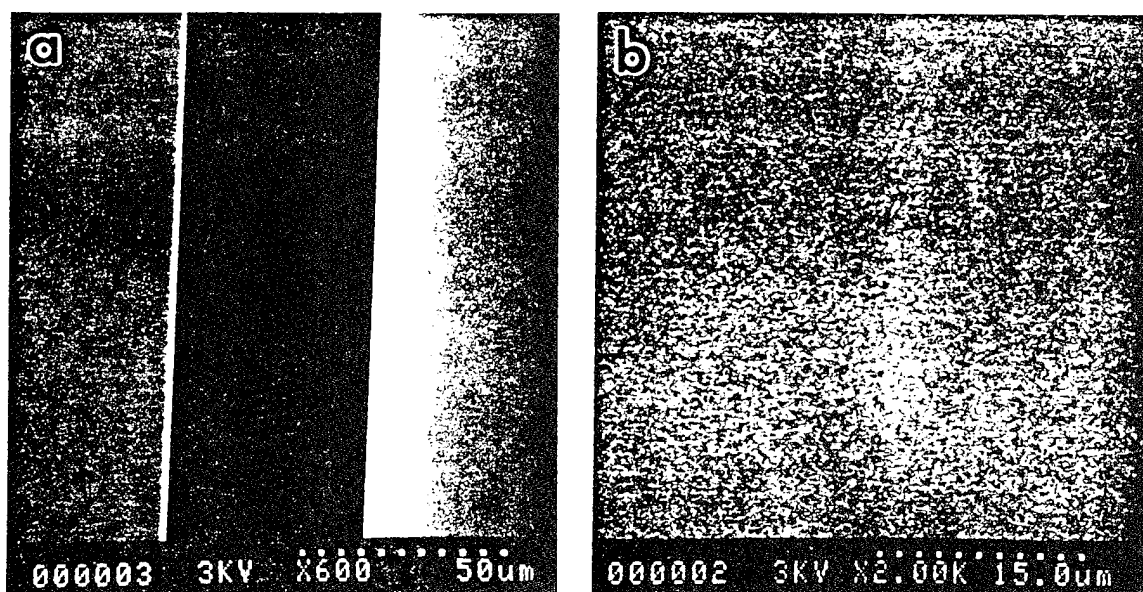


Fig. 2 SEM micrographs of (a) joint region after 4 hours ($\sim 2\mu\text{m}$) of homoepitaxial growth. The $50\mu\text{m}$ gap has been narrowed by approximately $2\mu\text{m}$. The surface topography (b) is excellent.

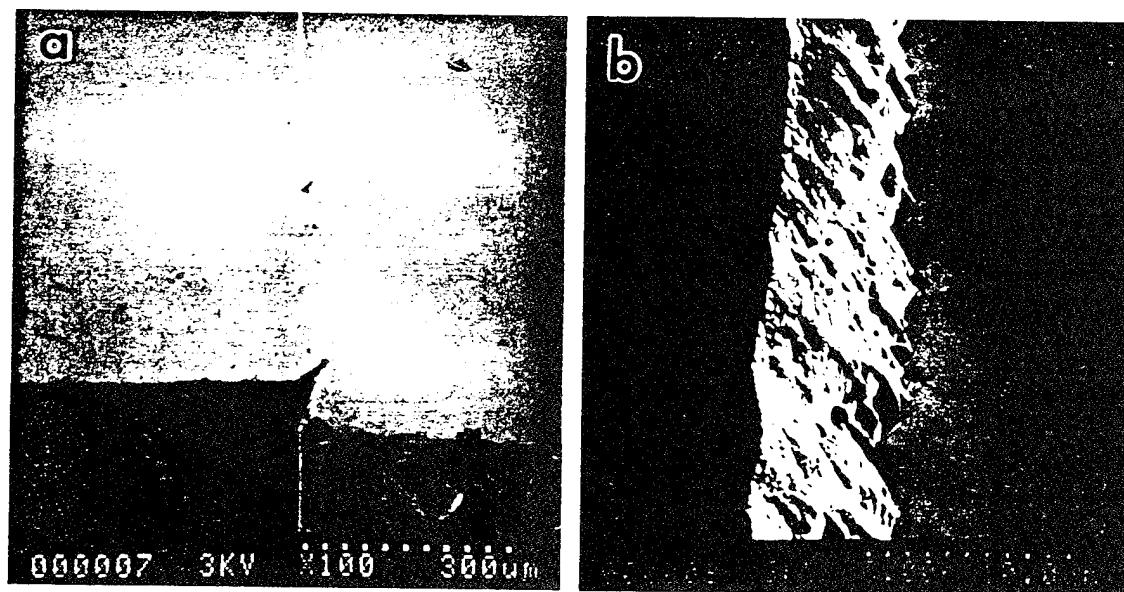


Fig. 3 SEM micrographs of epitaxially joined diamonds. (a) A low magnification view shows the joint region. The gap has been completely closed. (b) A closer view shows the joint with a $\sim 6\mu\text{m}$ vertical step.

The role of hydrogen on the enhancement of secondary electron emission from C(001)

T.P. Humphreys, R.E. Thomas, D.P. Malta, J.B. Posthill, M.J. Mantini, R.A. Rudder,
G.C. Hudson and R.J. Markunas

Research Triangle Institute, Research Triangle Park, North Carolina 27709-2194.

Abstract

Complementary spectroscopy techniques of ultraviolet photoemission and secondary electron emission have been employed to investigate the role of chemisorbed hydrogen in the enhancement of low-energy electron emission from natural type IIb C(001) diamond surfaces. Following H-plasma exposure, an intense low-energy emission peak was observed with both spectroscopies. The emission intensity associated with the chemisorbed hydrogen was found to be a direct function of surface coverage and independent of surface reconstruction. The presence of a discrete hydrogen induced unoccupied state, near the conduction band edge, from which low-energy inelastically excited electrons can escape is believed to account for the low-energy emission peak.

Submitted to

Applied Physics Letters

To date, photoemission studies from the as-polished (a process which includes polishing the diamond single crystal on an Fe wheel with olive oil) and hydrogen plasma exposed C(111) natural diamond surfaces have been shown to exhibit negative electron affinity (NEA).¹⁻³ In particular, van der Weide and Nemanich have recently reported a low-energy emission peak in the ultraviolet photoemission spectrum (UPS) from a hydrogen plasma-exposed C(111) surface which they attribute to NEA.³ In contrast a similar peak has also been observed in the UPS spectrum from the C(001) surface upon annealing at 1035°C.⁴ Moreover, Pate, et al., have suggested from an analysis of the oscillatory structure in the total electron yield measurements from the as-polished C(111) 1x1:H surface, that the low-energy emission feature is a result of exciton induced electron emission.^{5,6} Recently, Malta, et al., using scanning electron microscopy have reported that a significant enhancement in secondary electron emission is observed from hydrogen plasma-treated natural type IIa or type IIb C(001)-1x1 surfaces.⁷

In this letter, the role of chemisorbed hydrogen and its influence on the enhancement of low-energy secondary electron emission from type IIb C(001) surfaces is examined using (UPS) and secondary electron emission spectroscopy (SEES).

The SEES technique has been previously employed by Hoffman, et al.,⁸ to map the density of unoccupied conduction band (CB) states for a type IIa C(110) diamond surface. In this technique the energy distribution of emitted electrons is predominately a function of the density of final (CB) states. In contrast, the emission features in the photoemission technique are largely determined by the contribution of the joint density of initial and final (CB) states which are superimposed on a background of low-energy inelastically scattered electrons. Hence, a comparison of the corresponding SEES and UPS spectra enables unambiguous identification of the final state contribution in the observed photoemission spectrum.

Commercially supplied low-resistivity $3 \times 3 \times 0.25$ mm semiconducting natural diamond, type IIb, C(001) substrates were chemically cleaned in boiling solutions of chromic acid and aqua-regia. Samples for UPS studies were hydrogenated by rf-plasma

H-exposure for 1 min at 50 W power at a temperature of 380°C and a hydrogen pressure of 7 mT. Samples were then transferred *in vacuo* to the UPS facility. The UPS spectra were recorded in the angle-integrated mode using a He I ($h\nu = 21.2$ eV) light source with the energy analyzer at normal incidence (energy resolution, $\Delta E \sim 0.2$ eV). A sample bias of -1 V with respect to the analyzer was used for UPS analysis. SEES measurements were performed in a separate UHV analytical chamber equipped with a Perkin-Elmer C10-155 single pass CMA for energy analysis of the emitted electrons. A primary electron beam energy of 150 eV with a beam current of ~ 1 μ A was utilized. A sample bias of -2 V with respect to the analyzer was used for SEES studies. *In situ* atomic hydrogen was supplied by flowing hydrogen over a 1700°C tungsten filament. Sample temperatures were measured by a Cr-Al thermocouple spot welded to the heater adjacent to the diamond. Samples for SEES studies were plasma treated under the identical conditions as those employed in the UPS studies but were subsequently air transferred to the SEES facility.

Shown in Fig. 1 are the corresponding UPS and SEES spectra obtained from the thermally clean and hydrogen terminated C(001) surface. Because of the small size of the diamond samples, bulk photoemission peaks from a Pt mask are also superimposed on the diamond spectra. However, these Pt features have been observed in the present study to occur at higher kinetic energies, typically above ~ 13 eV, and do not interfere with the low-energy emission or secondary electron region of interest in this analysis. Accurate determination of the position of the diamond valence band edge (VBE) has been obtained by background subtraction of the corresponding Pt features in the spectra. In our experiments the VBE for the 900°C annealed sample is located 8.2 eV above the prominent bulk emission feature in Fig. 1(a) which occurs at ~ 10.1 eV. Previous studies by van der Weide and Nemanich have also reported similar results for the clean C(001) surface.⁴ The UPS spectrum obtained after hydrogen-plasma exposure clearly shows an intense low-energy emission peak at ~ 1.7 eV, Fig. 1(b). Also evident is the corresponding decrease in the low-energy cutoff edge which results in an increase in the

width of the photoemission spectrum. Additionally, there is a ~ 0.2 eV shift in the spectrum to higher kinetic energies which would suggest the formation of a surface dipole indicative of an electropositive hydrogen terminated surface.⁹ A spectral width of ~ 16.6 eV has been determined from the energy difference between the low-energy peak position and the onset of emission at the VBE. Evidently, the width of the emission spectrum is greater than the calculated width of 15.73 eV which is given by $h\nu - E_g$, where $E_g = 5.47$ eV¹⁰ is the indirect band gap. In this expression, the bulk band gap defines the energy position of the conduction band minimum (CBM) relative to the valence band emission edge, which results in the CBM appearing at the low-energy cutoff emission edge in the UPS spectrum. A shift in the cutoff emission edge to lower energy effectively reduces the bandgap. To account for this apparent bandgap reduction, it is proposed that hydrogen induces an unoccupied state ~ 0.9 eV below the CB edge. In consequence, secondary electrons which are photoexcited into the CB can scatter into this unoccupied hydrogen induced state. The subsequent escape of these electrons into the vacuum gives rise to the observed low-energy emission peak.

Corresponding SEES analysis of the hydrogen terminated surface shows the presence of an identical low-energy emission feature at ~ 1.7 eV, Fig. 1 (d). In order to align the energy positions of the low-energy and bulk emission features in the SEES and the UPS spectra, the SEES spectra have been shifted to lower kinetic energies by 0.5 eV. This energy shift takes into account the differences in analyzer work functions and biasing conditions employed in the separate experiments. The presence of the low energy emission peak in the SEE spectrum corroborates the conclusion that the emission is from a state induced near the CB edge. This state is located ~ 0.7 eV below the CB edge in the SEES spectra and compares favorably with the measured value obtained from photoemission. Further, it has also been observed that the low-energy emission peak in the UPS and SEES spectra can be removed upon annealing to approximately 900°C.

The intensity of the secondary emission feature was also investigated with SEES as a function of hydrogen dose as shown in Fig. 2. The dose versus intensity studies were

performed after the sample had received an anneal at 1050°C at which point the low-energy electron diffraction (LEED) pattern showed a 2x1 surface reconstruction. This LEED pattern was unchanged before and after atomic hydrogen exposures by *in situ* hot filament dosing. The intensity response is initially linear with hydrogen dose and then the secondary electron emission starts to saturate. Also shown in Fig. 2 are measurements of hydrogen thermal desorption intensities as a function of hydrogen dose. The thermal desorption data points represent data taken in previous experiments where peak areas for hydrogen desorption from the C(100)-2x1:H surface were integrated to obtain an intensity value.¹¹ By comparing the two responses it is apparent that the secondary electron emission intensity is a simple function of surface hydrogen coverage.

Secondary electron emission results obtained during cycles of annealing to 900°C followed by cooling and hydrogenation are very consistent through multiple repetitions. However, in addition to reconstructing the surface to a 2x1 configuration, annealing at 1050°C also produced subtle changes in the SEES spectra. Examples are given in Fig. 3 of spectra obtained from clean surfaces of samples annealed at 900°C for 60s and at 1050°C for 60s and for both samples after *in situ* hot filament hydrogen dosing for 600s at 2×10^{-7} T. After annealing at 1050°C the clean surface has an emission onset at 2.8 eV, Fig. 3(d), compared to an emission onset of 1.6 eV for the clean surface after annealing at 900°C, Fig. 3(c). Following rehydrogenation both surfaces still exhibited narrow, intense secondary electron emission peaks at 1.7 eV, however, from Figs. 3(a) and 3(b) it is evident that the emission from the 1.7 eV peak has been reduced on the sample which received the 1050°C anneal, Fig. 3(b). Also observed following the 1050°C anneal and hydrogenation is the appearance of a second hydrogen induced peak at approximately 2.5 eV, Fig. 3(b). Extended UHV hydrogen dosing of the surface annealed at 1050°C does not restore the original intensity of the 1.7 eV peak or remove the peak observed at 2.5 eV. However, re-exposure of the surface to the hydrogen plasma restores the 1x1 LEED pattern, removes the peak at 2.5 eV and restores the intensity of the peak at 1.7 eV.

The intensity and peak changes in the SEES spectra observed upon annealing at 1050 °C are coincident with a surface reconstruction from the 1x1 structure to the 2x1 structure that we observe with LEED. The plasma treated surface has a 1x1 LEED pattern and is thought to contain a high proportion of the dihydride structure. Given the steric constraints for hydrogen addition to the surface though, it is likely that the surface has not been completely converted from the monohydride structure.¹² Annealing at 900°C removes the hydrogen from the surface by desorption,¹¹ however, the surface does not fully reconstruct to the 2x1 configuration, as evidenced by LEED. Unoccupied surface states associated with the unreconstructed surface are then revealed at the leading edge of the electron emission spectra. Annealing at 1050°C results in a 2x1 LEED pattern and removes these surface states. The unoccupied surface states on the unreconstructed clean surface extend into the bandgap, in the same manner as the hydrogen induced states, which effectively reduces the bandgap of the diamond. In this case by approximately 1.2 eV. Dimer formation upon annealing also reduces the number of available hydrogen bonding sites on the surface and hence the emission intensity following rehydrogenation. The origin of the second emission peak that appears at 2.5 eV upon hydrogenation is less clear. It appears that reconstruction of the surface leads to the creation of two distinct sites for hydrogen bonding from which emission can occur. The steric constraints may lead to a condition where dimers are singly occupied by hydrogen. Finally, the inability of *in situ* hot filament hydrogen dosing to restore the SEES spectra to the state observed following plasma treatment is consistent with previous work which showed that atomic hydrogen fluences achieved with a hot filament under UHV dosing condition, i.e. $\sim 1 \times 10^{-5}$ T were insufficient to convert the 2x1 surface structure to the 1x1 configuration.¹³

In summary, it has been demonstrated by UPS and SEES that hydrogen plasma exposure of a C(001) surface results in the presence of an intense low-energy peak due to chemisorbed hydrogen. In particular, the emission peak intensity associated with the chemisorbed hydrogen is a direct function of hydrogen surface coverage, and independent of surface reconstruction. The presence of a hydrogen induced unoccupied state below

the CB edge from which low-energy inelastically excited electrons can escape is believed to account for the observed low-energy electron emission feature.

The financial support of the Ballistic Missile Defense Organization/Innovative Science and Technology Office through the Office of Naval Research (Contract No. N00014-92-C-0081) is gratefully acknowledged.

References

1. F.J. Himpsel, J.A. Knapp, J.A. van Vechten and D.E. Eastman, Phys. Rev. B **20**, 624 (1979).
2. B.B. Pate, M.H. Hecht, C.Binns, I. Lindau and W.E. Spicer, J. Vac. Sci. Technol. **21**, 268 (1982).
3. J. van der Weide and R.J. Nemanich, Appl. Phys. Lett. **62**, 1878 (1993).
4. J. van der Weide and R.J. Nemanich, Phys. Rev. B **49**, 13629 (1994).
5. B.B. Pate, I. Lindau and W.E. Spicer, Proceedings of the 17th International Conference on the Physics of Semiconductors, edited by J.D. Chadi and W.A. Harrison (Springer Verlag, 1985) 1201.
6. C. Bandis, D. Haggerty and B.B. Pate, Mat. Res. Soc. Symp. Proc. 339,75 (1994).
7. D.P. Malta, J.B. Posthill, T.P. Humphreys, R.E. Thomas, G.G. Fountain, R.A. Rudder, G.C. Hudson, M.J. Mantini, and R.J. Markunas, Appl. Phys. Lett. **64**, 1929 (1994).
8. A. Hoffman, M. Folman and S. Praver, Phys. Rev. B **44**, 4640 (1991).
9. W.L. Jolly, 'Modern Inorganic Chemistry', (McGraw-Hill Book Company, New York, (1984)), pp. 71 - 76.
10. C.D. Clark, P.J. Lightowlers and D.R. Wright, Proc. R. Soc. London Ser. A **277**, 312 (1964).
11. R.E. Thomas, R.A. Rudder and R.J. Markunas, J. Vac. Sci. Technol. **10**(4) 2451, (1992).
12. Y.L. Yang, L.M. Struck, L.F. Sutco and M.P. D'Evelyn, Thin Solid Films. **225**, 203, (1993).

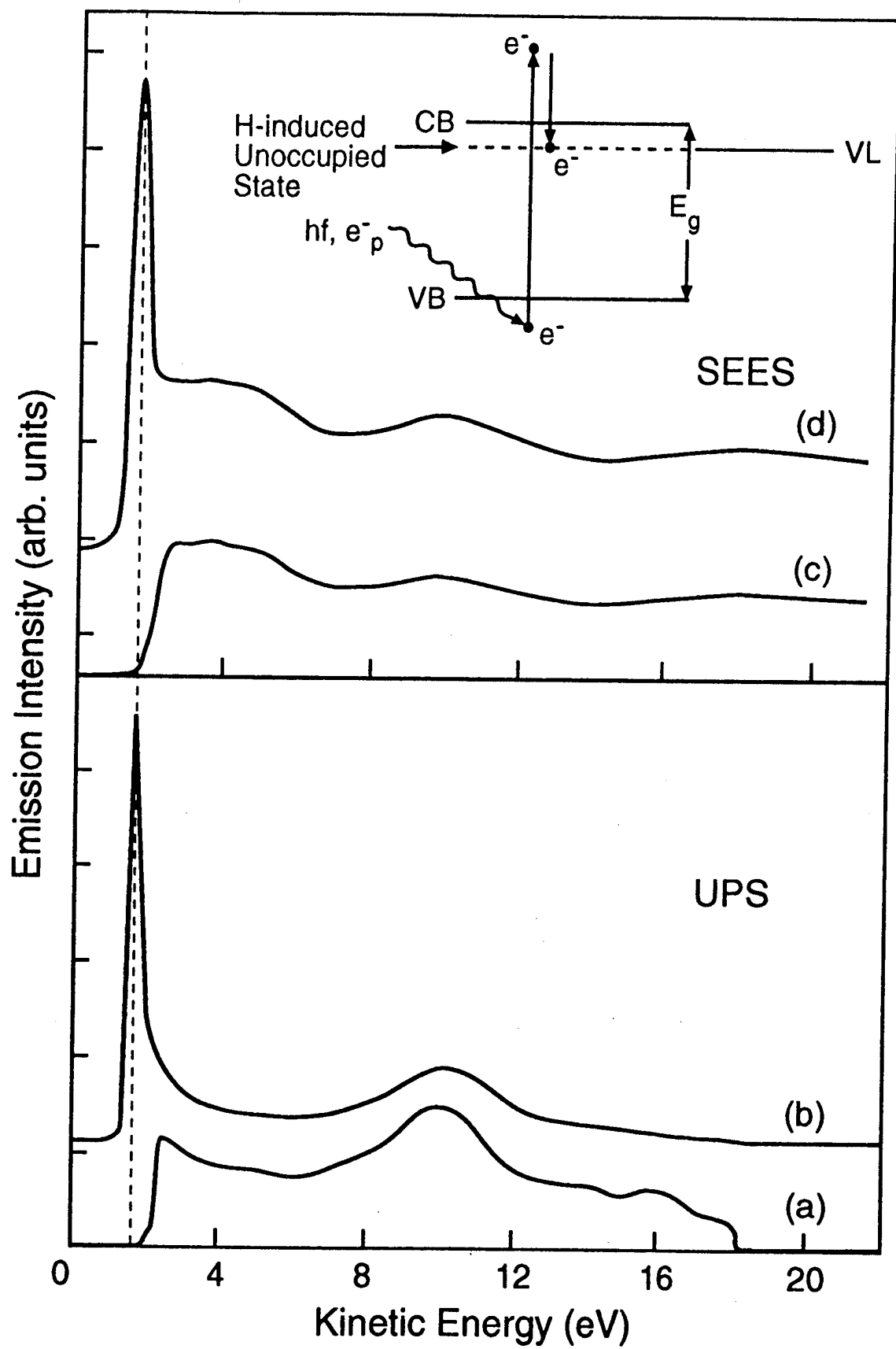
13. R.E. Thomas, R.A. Rudder, R. J. Markunas, D. Huang and M. Frenklach, J. Chem. Vap. Deposition. **1**, 6 (1992).

Figure Captions

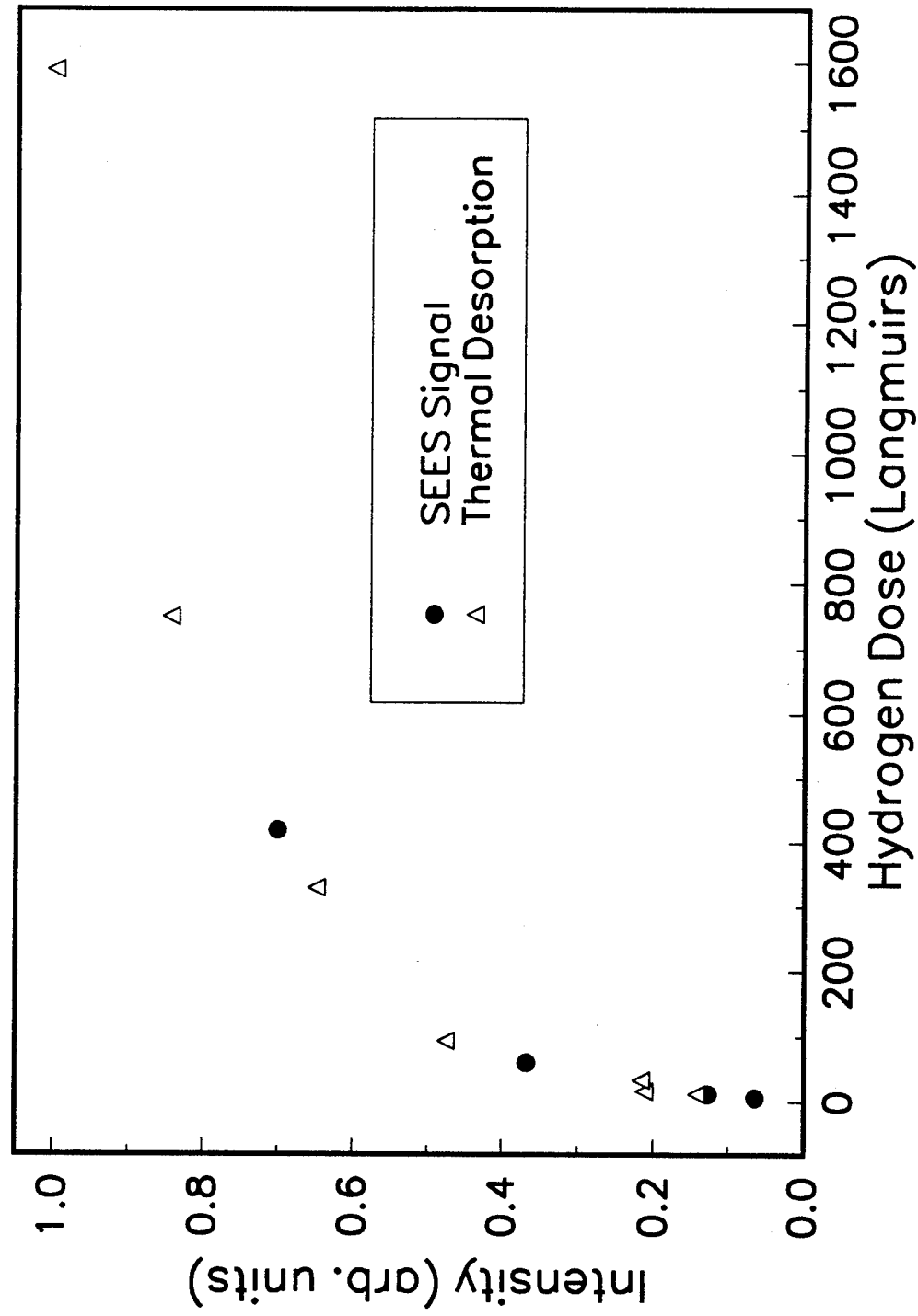
Fig. 1 Corresponding UPS and SEES spectra from the 900°C annealed (a) and (c), and hydrogen terminated (b) and (d), C(001) surface. Insert shows a schematic representation of the low-energy electron emission process.

Fig. 2 Comparison of coverage dependence of hydrogen thermal desorption intensity and secondary electron emission intensity. Both curves were normalized.

Fig. 3 SEES spectra comparing samples annealed at 900°C and 1050°C followed by hydrogenation.



ELECTRON EMISSION INTENSITY VS HYDROGEN DOSE



COMPARISON OF CLEAN AND HYDROGEN TERMINATED SURFACES

